DEPARTMENT OF PHYSICS
UNIVERSITY OF JYVÄSKYLÄ
RESEARCH REPORT No. 12/2011

Ca-P-O thin film preparation, modification and characterisation

A.R. Ananda Sagari

Academic Dissertation
for the Degree of
Doctor of Philosophy

*To be presented, by permission of the
Faculty of Mathematics and Natural Sciences
of the University of Jyväskylä,
for public examination in Auditorium FYS–1 of the
University of Jyväskylä on December 16, 2011
at 12 o'clock noon*

Jyväskylä, Finland
December 2011

Acknowledgment

Rise of this thesis wouldn't have been possible without the support and encouragement of many people. My sincere wholehearted gratitude for each and every helping hands in one way or the other.

The journey through my PhD studies has been nurtured by two supervisors Prof. Harry J. Whitlow and Adj. Prof. Timo Sajavaara.

I am indebted to Harry for bringing me into the world of PhD studies and providing me with an opportunity to do my research in such an interesting field. Things would not have been possible without the efforts Harry had taken to set the stage for me to start. Harry is a very cheerful and a dynamic person who has always been my father figure, channeling me in the right directions. Thank you for all the suggestion, discussions and much needed guidance throughout all the years.

Timo, my sincere thanks for being extremely patient towards me, for every time I stepped in with millions of questions. For all the sound advice, unstinted help and molding me, for which I will ever remain grateful. Timo, is a perfectionist, positive and a very hard working person who played a major role in raising my bar in terms of a scientific career, giving me freedom to explore and learn. Timo is like a big brother who has been caring and supportive right from day one.

My special thanks to Dr. Sergey Gorelick, Mikko Laitinen for their great company as colleagues. Sergey has been motivating by his own methods and kept the environment extremely cheerful. Mikko, who has been generously kind while dealing with technical, practical difficulties both in and out of the lab. He never retrained himself in checking if everything is ok.

I wish to thank two good friends Dr. Liping Wang and Dr. Elisabeth Wieslander for all the cheerful moments we have spent together at work and pleasant discussions around the coffee table. Thanks are also due to Claire Lautaret, Dr. Nitipon Puttaraksa and Rattanaporn Norarat for being helpful when in need, pleasant discussion and good company. Thanks also to Laura Mättö, Jaakko Julin and Mari Napari for pleasant company and help. I extend my sincere thanks to Paavo Rahkila, Dr. Ma Hongqiang, Jari Malm, Prof. Matti Putkonen, Adj. Prof. Manu Lahtinen and Prof. Sulin Cheng for all their help during course of this study.

I would also like to thank the Head of the Physics Department, Prof. Jukka Maalampi, Prof. Rauno Julin, Head of the Accelerator Laboratory and whole of the Physics Department for creating such a warm and friendly working atmosphere. I particularly remain grateful to Antti Nuottajärvi and Tarmo Suppula for technical help at clean room facility, Nanoscience Centre.

My thanks to Soili Leskinen, Anna-Liisa Blå and Ritva Väyrynen for their help with

all the administrative matters. A special thanks to Marjut Hilska for not only helping me at work but also being very friendly, making me experience real Finnish food and adventures.

The financial support from the Department of Physics of University of Jyväskylä, the Graduate School of Particle of Nuclear Physics (GRASPANP), the Centre of Excellence in Nuclear and Accelerator based Physics and the Centre for International Mobility (CIMO) is gratefully acknowledged. I am thankful to Magnus Ehrnrooth, Vilho, Yrjö ja Kalle Väisälä foundation, for the financial support that enabled me to travel and participate in international conferences.

Finally I would like to thank my families both in Finland and India. I will always be thankful to my Indian friends here for their help during the time of need and warm company all throughout the years. Special thanks to Shanthi, Vinoo, Merie, Asima, Rtitka and Rupa for great friendship and mutual encouragement. My heartfelt thanks to Dr. Somjai Sangyuenyongpipat and Tero Isotalo for being not only as friends but also taking in me as part of their family. My warm thanks to my Finnish God parents Mrs. Birgitta von Bonsdorff and Dr. Henrik von Bonsdorff, who have given parental warmth, treating me as their little one. My warm thanks to my grandparents and extended family, who staying thousands miles away reached me through their thoughts. My heartfelt thanks to Subbu Anna, Jhiju and Sundari who undoubtedly showered me with their unconditional love, support and believing in me during tough days. Thanks will be too little word to Mom and Papa for bringing me to this world and for making me what I am today. You both are my pillars of strength.

Jyväskylä, December 2011
Ananda Rajashekar

Abstract

Bioceramics are biocompatible ceramic materials, that interact with biological systems of the body to treat, strengthen or replace body functions. Most conventional bioceramics are oxide ceramics, glass ceramics and calcium phosphate ceramics. Among these calcium phosphates, synthetic hydroxyapatite has been extensively studied due to its biomimetic properties similar to that of natural bone. One approach to prepare synthetic hydroxyapatite is to first deposit amorphous Ca-P-O thin film and then by means of post deposition annealing initiate the formation of hydroxyapatite crystals to the film. In addition to the correct film composition and crystalline structure, other surface properties such as wettability and surface nano- and microtopography are very significant for the biocompatibility.

In this study Ca-P-O thin films were deposited using two different techniques, ion beam sputtering and atomic layer deposition (ALD). Films deposited using both techniques were amorphous after deposition. For sputter deposited films, the Ca/P atomic ratio determined by means of ion beam analysis approached stoichiometric hydroxyapatite when hydroxyapatite powder doped with extra phosphorous was used as the sputtering target. Though the sputtered films showed good biocompatibility in cell attachment studies, the dissolution of as-deposited films in cell culture medium is a disadvantage. The surface of as-deposited and annealed thin films deposited using ALD were locally modified by high and low energy irradiation. After low energy ion irradiation the as-deposited films showed an increase in hydrophilicity, which was determined using contact angle measurements, and also greater spreading of mouse pre-osteoblast cells.

The effect of surface topography was studied by abrading Ti metal substrates to different roughnesses before depositing 2–50 nm thick ALD Ca-P-O films on them. Ti was selected in order to combine the biocompatibility of Ca-P-O thin-films with the mechanical strength of the Ti metal substrate. Ca-P-O films deposited on smoother substrates showed higher Ca/P atomic ratios than those on the rough substrates, demonstrating the influence of roughness on the film growth during the deposition. As-deposited Ca-P-O films acted as equally good cell culture substrate as untreated Ti samples used as a control.

After post deposition annealing at 800 °C, Ca-P-O films were crystallized on Si substrates and showed filopodic morphology of pre-osteoblast cells. Films on Ti showed also filopodic morphology of cells after 700 °C annealing but at 800 °C the number of cells substantially dropped, most likely due to formation of a less biocompatible TiO_2 rutile phase on the surface.

Abstract in Hindi

हाल पारंपरिक जैव चीनी मिट्टी की चीज़ें ऑक्साइड सिरेमिक कांच चीनी मिट्टी की चीज़ें और कैल्शियम फॉस्फेट चीनी मिट्टी की चीज़ें हैं । इन कैल्शियम फॉस्फेट के अलावा विशेष रूप से हैयडराखसीआपाटथटठ अपने भाथौमिमीटिकस प्राकृतिक हड्डी के समान गुणों की वजह से अध्ययन किया गया है । एक सिंथेटिक हैयडराखसीआपाटथटठ तैयार दृष्टिकोण पहले जमा अनाकार कैल्शियम फॉस्फेट ऑक्सीजन पतली फिल्म के लिए है और फिर पोस्ट बयान उच्च तापमान उपचार के माध्यम से फिल्म के लिए हैयडराखसीआपाटथटठ क्रिस्टल के गठन आरंभ। सही फिल्म संरचना और क्रिस्टलीय संरचना के अलावा यह भी वेटाटबिलिटी और नैनो और मौकरौटेमौगारफी की सतह के रूप में सतह के गुणों भाथौखामपाटबिलिटी के लिए बहुत महत्वपूर्ण हैं ।

इस अध्ययन कैल्शियम फॉस्फेट ऑक्सीजन में पतली फिल्मों दो विभिन्न तकनीकों आयन बीम सापटारिग और परमाणु परत बयान का उपयोग कर जमा थे । फिल्म्स दोनों तकनीकों का उपयोग करते हुए बयान के बाद अनाकार थे जमा । के लिए धूम फिल्मों जमा फॉस्फोरस परमाणु आयन बीम विश्लेषण के माध्यम से निर्धारित अनुपात में कैल्शियम साटठियौमटारीक हैयडराखसीआपाटथटठ के पास जब हैयडराखसीआपाटथटठ पाउडर के साथ डैबाठ अतिरिक्त फॉस्फोरस सापटारिग लक्ष्य के रूप में इस्तेमाल किया गया था । हालांकि सापटारैह फिल्मों सेल लगाव पढ़ाई में अच्छा भाथौखामपाटबिलिटी दिखाया सेल संस्कृति माध्यम के रूप में जमा फिल्मों के विघटन के एक नुकसान है । के रूप में जमा है और उच्च तापमान संसाधित पतली फिल्मों की सतह जमा परमाणु परत बयान का उपयोग स्थानीय रूप से उच्च और कम ऊर्जा विकिरण द्वारा संशोधित किया गया है । कम ऊर्जा आयन विकिरण के बाद के रूप में जमा फिल्मों थडौफीलिसिटी जो संपर्क कोण माप का उपयोग कर निर्धारित किया गया था में वृद्धि देखी गई और भी अधिक से अधिक प्रसार ।

सतह स्थलाकृति का प्रभाव उन पर बीस पचास नैनो मीटर मोटी परत परमाणु बयान कैल्शियम फॉस्फेट ऑक्सीजन फिल्मों जमा से पहले विभिन्न राफानास टाइटेनियम धातु साभसटैठस आबरेडिंग द्वारा अध्ययन किया गया था । टाइटेनियम चुना गया था क्रम में टाइटेनियम धातु सब्सट्रेट के यांत्रिक शक्ति के साथ गठबंधन करने के लिए कैल्शियम फॉस्फेट ऑक्सीजन पतली फिल्मों के भाथौखामपाटबिलिटी । कैल्शियम फॉस्फेट ऑक्सीजन चिकनी साभसटैठस पर जमा फिल्मों किसी न

किसी साभसटैठस पर उन लोगों की तुलना में फॉस्फोरस परमाणु अनुपात करने के लिए उच्च कैल्शियम से पता चला है खुरदरापन के बयान के दौरान फिल्म के विकास पर प्रभाव दिखा । के रूप में जमा कैल्शियम फॉस्फेट ऑक्सीजन फिल्मों अनुपचारित टाइटेनियम एक नियंत्रण के रूप में इस्तेमाल किया नमूने के रूप में भाथौखामपाटबिलिटी दिखाया भी उतना ही अच्छा । आठ सौ ग पर पोस्ट बयान उच्च तापमान प्रक्रिया के बाद कैल्शियम फॉस्फेट ऑक्सीजन फिल्मों सी साभसटैठस पर सघन थे और इन भाथौखामपाटबिलिटी दिखाया बहुत अच्छा । टाइटेनियम पर फिल्म्स अत्यधिक सात सौ ग के बाद लेकिन आठ सौ पर उच्च तापमान प्रक्रिया के बाद अभी भी थे भाथौखामपाटाबल ग भाथौखामपाटबिलिटी काफी गिरा दिया सबसे कम भाथौखामपाटाबल सतह पर रूटाइल टाइटेनियम डाइऑक्साइड चरण के गठन के कारण होने की संभावना।

Author's address A.R. Ananda Sagari
Department of Physics
University of Jyväskylä
Finland

Supervisors Adj. Prof. Timo Sajavaara
Department of Physics
University of Jyväskylä
Finland

Prof. Harry J. Whitlow
Department of Physics
University of Jyväskylä
Finland

Pre-examiners Prof. Anders Hallén
ETK Components and Circuits
Royal Institute of Technology
Kista
Sweden

Prof. Jari Koskinen
Department of Materials Science and Engineering
Aalto University
Finland

Opponent Dr. John E.E. Baglin
Senior Researcher
IBM Almaden Research Center
San Jose, California
United States of America

List of Publications

The main results of this thesis have been reported in the following publications (the author contributions are in the parentheses).

[Paper I] *Ion-sputter deposition of Ca-P-O films for microscopic imaging of osteoblast cells.* A.R.A. Sagari, C. Lautarent, S. Gorelick, P. Rahkila, M. Putkonen,K. Arstila, T. Sajavaara, S. Cheng, H.J. Whitlow. Nucl. Instr. and Meth. B 261 (2007) 719. (Preparation of thin films, investigation of the data, principal author.)

[Paper II] *Wettabilty and compositional analysis of hydroxyapatite films modified by low and high energy ion irradiation.* A.R.A. Sagari, P. Rahkila, M. Väisänen, R. Lehto, T. Sajavaara, S. Gorelick, M. Laitinen, M. Putkonen, S. Sangyuenyongpipat, J. Timonen, S. Cheng, H.J. Whitlow. Nucl. Instr. and Meth. B 266 (2008) 2515. (Irradiation of samples, participated in contact angle measurement, AFM characterisation, data analysis, principal author.)

[Paper III] *Influence of titanium-Substrate roughness on Ca-P-O thin films grown by atomic layer deposition.* A.R.A. Sagari, J. Malm, M. Laitinen, P. Rahkila, M. Hongqiang, M. Putkonen, M. Karppinen, H.J. Whitlow, T. Sajavaara. Manuscript. (Sample preparation, TOF-ERDA measurements, data analysis, AFM characterisation, principal author.)

[Paper IV] *Efect of annealing on surface properties, composition and biocompatibility for atomic layer deposited Ca-P-O films on titanium and silicon substrates.* A.R.A. Sagari, J. Malm, M. Laitinen, P. Rahkila, M. Lahtinen, M. Hongqiang, M. Putkonen, M. Karppinen, H.J. Whitlow, T. Sajavaara. Manuscript. (Sample preparation, TOF-ERDA measurements, data analysis, AFM characterisation, principal author.)

Other work to which author has contributed: (Not included in thesis)

Growth of bone-cells on lithographically modified surfaces. S. Gorelick, P. Rahkila, A.R.A. Sagari, T. Sajavaara, S. Cheng, L. B. Karlsson, J. A. van Kan, H.J. Whitlow. Nucl. Instr. and Meth. B 260 (2007) 130.

Mobility determination of lead isotopes in glass for retrospective radon measurements. M. Laitinen, I. Riihimäki, J. Ekman, A.R.A. Sagari, L.B. Karlsson, S. Sangyuenyongpipat, S. Gorlick, H. Kettunen, H. Penttilä, R. Hellborg, T. Sajavaara, J. Helgesson, H.J. Whitlow. Radiat. Prot. Dosim. 131 (2008) 212.

Development of micro-contact printing of osteosarcoma cells using MeV ion beam lithography S. Sangyuenyongpipat, V. Marjomäki, S. Ikonen, T. Sajavaara, A.R.A. Sagari, S. Gorelick, M. Laitinen, H.J. Whitlow. Nucl. Instr. and Meth. B 267 (2009) 2306.

Contents

1 Introduction 1

2 Thin films and titanium as biomaterials 5
2.1 Ca-P-O thin films 5
2.2 Role of biomaterials in implantation 6
2.2.1 Interface details 6
2.3 Titanium as implant material 7
2.3.1 Modification of surface morphology 8

3 Thin film deposition and modification 9
3.1 Sample preparation 9
3.1.1 Borosilicate and Si substrates 9
3.1.2 Titanium substrate 9
3.2 Sputtering target preparation 11
3.3 Ca-P-O thin film deposition 11
3.3.1 Ion sputtering 11
3.3.2 Sputter deposition at JYFL 14
3.3.3 Atomic layer deposition 15
3.3.4 Ca-P-O Parameters for ALD deposition 17
3.4 Ion interaction with materials 17
3.5 High energy irradiation 19
3.5.1 Tandem Pelletron accelerator 19
3.5.2 Programmable Proximity Aperture Lithography 19
3.5.3 Irradiation parameters 20
3.6 Low energy irradiation 21
3.6.1 Ion irradiation system 21
3.6.2 Irradiation parameters 22

4 Sample characterisation 23
4.1 Rutherford Backscattering Spectrometry 24
4.1.1 RBS measurements 24
4.2 Elastic Recoil Detection Analysis 24
4.2.1 TOF–ERDA measurements 25
4.3 Atomic Force Microscopy 26
4.3.1 AFM measurement details 27
4.4 X-ray diffraction 28

4.5 X-ray diffraction measurement details 28
4.6 Surface wettability 29
4.6.1 Contact angle measurements 29
4.7 In vitro cell studies 30
4.7.1 Cell culture experiments 30

5 Experimental results and discussion 33
5.1 Composition of Ca-P-O thin film 33
5.1.1 Atomic layer and sputter deposited films 33
5.1.2 Annealing 35
5.1.3 Ion irradiation 36
5.1.4 Substrate roughness 36
5.2 Surface morphology 37
5.2.1 Annealing 37
5.2.2 Ion irradiation effect 39
5.3 Hydrophilicity 40
5.4 Crystalline phases 41
5.5 Cell growth and cell morphology 42

6 Conclusions 45

1 Introduction

One of the major concerns in the field of osteology is bone fragility, i.e. osteoporosis. The mineral phase, which is the main constituent of bone, is calcium phosphate, and osteoporosis is characterised by gradual loss of calcium in bone leading to a very porous and weak bone, thereby causing bone fracture. The natural and accidental bone fracture or degradation is often treated by bone substitutions. A continuous state of resorption and remodeling after bone implant initiates the healing process. *Resorption* is where osteoclast cells absorb bone matter and *remodeling* is where osteoblast cells produce new bone. Changes in the dynamics equilibrium between these two process allows bone to grow and change shape. The rate of resorption of bone substitutes depends on composition, porosity and the geometry of the biomaterial used.

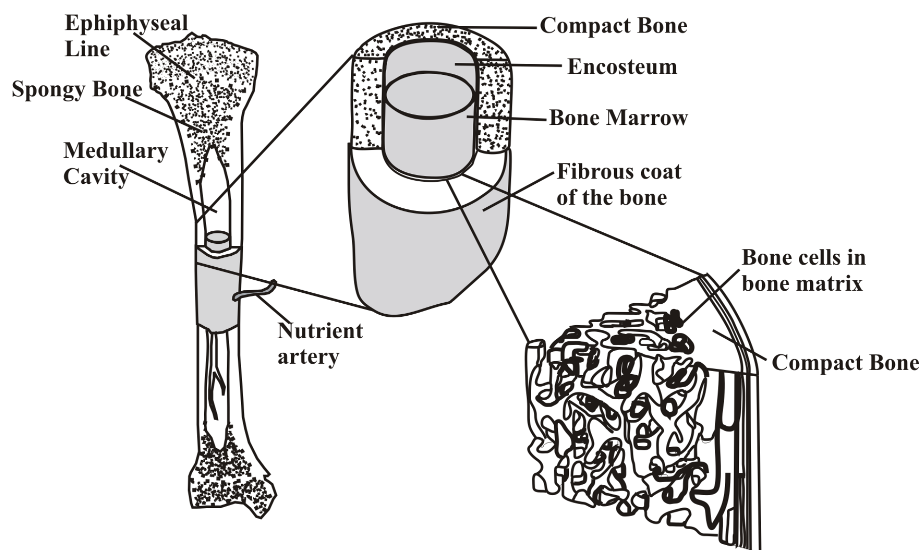

Figure 1.1: Section of human bone.

A cross-section of human bone is shown in Fig. 1.1. The most widely used biomaterials for bone substitute and bone implant are calcium phosphate ceramics. Ceramics are materials of inorganic nature that are brittle but advanced ceramics with their great biological tolerability are used to create components suitable for replacement in the human body. Bioceramics range in biocompatibility from the ceramic oxides, which are inert in the body to other resorbable materials. The most conventional bio-ceramics for implants are 1) oxide ceramics such as aluminium oxide (Al_2O_3), zirconium oxide (ZrO_2), 2) glass ceramics and 3) calcium phosphate ceramics such as hydroxyapatite

Material	Youngs Modulus /(GPa)	Bend Strength /(MPa)	Tensile Strength /(MPa)	Density /(gcm^{-3})
Bone	10–20	160	124–174	1.6
HA	70–120	20–80	40–100	3.156

Table 1.1: Physical properties of bone and hydroxyapatite (HA) [13–16].

(HA, chemical formula $Ca_{10}(PO_4)_6(OH)_2$), tricalciumphosphate (TCP) and biphasic calcium phosphates (BCP) [1–5]. The two main advantages of using ceramics as bone graft substitutes are that, there is no threat of disease transmission and there is an absence of inflammatory response. Additionally, calcium phosphate and HA display an osteoconductive property[1]. Better stabilisation of calcium phosphates and HA is obtained by increasing its crystallinity, which results in decrease of calcium and phosphate release from its surface and therefore lowering the rate of degradation [6].

The use of bulk calcium phosphate ceramics and HA is limited to non- or low-load bearing applications due to brittleness associated with low impact and fracture resistance. This can be directly seen from comparison of mechanical properties of bone and HA in Table 1.1. To eliminate this problem, it was suggested that quality of implants could be improved by depositing calcium phosphate on the metal implants with thin films. This approach would combine the mechanical strength of implant with the biological properties of calcium phosphate ceramics. The main function of calcium phosphate thin films for bone implant interface devices is to improve the long-term biocompatibility of metallic implants. For implants such as Co-Cr and stainless steel-based systems, calcium phosphate thin films form a barrier to inhibit corrosion and associated metal ion release by the metallic substrate in vivo [7–9]. Metal implants coated with calcium phosphate thin film are reported to exhibit rapid surface bone apposition with good stability [10–12].

Early research in the field of implants was on understanding the biomechanical properties of the metal used as implants. Critical factors for the success of implants depend on material selected, biocompatibility and design of material structure. Though metals and metal alloys reached many of the biomechanical requirements of surgical implants, the interface bonding between the metal implant and surrounding bone still tends to be the important factor for the success of the implants. Commonly used biocompatible metal implants are titanium, titanium alloys or stainless steel. Weak or poor interfacial bonding, formation of a non-adherent fibrous tissue layer and delamination of coating with formation of particle debris can to lead to implant failures [17–22].

Synthetic HA has been extensively used in experimental studies and in orthopedic

[1]the ability of the material to promote bone growth on its surface for the fixation of the implants.

surgery. Natural sources of calcium phosphate ceramics are from human or bovine bone or from coral, invertebrate marine organisms. Artificial calcium phosphate and HA can be synthesised from aqueous solution [23], by solid-state reaction [24] or by hydrothermal methods co-precipitation [25–27], sol-gel process [28] and other methods [29]. They differ from natural origins in composition, physical, chemical properties and crystal morphology depending on the method used for synthesis.

The critical factors to determine the quality of calcium phosphate coating are thickness, crystallinity, biocompatibility, adhesion to implants and wear resistance of the thin film. Dissolution and mechanical properties of coating depend on the thickness coating. The higher thermal expansion coefficient of HA than titanium alloy yields tensile stress which develops cracks through the coatings [30]. The disadvantage of using thick coatings are delamination, fragmentation and increase in residual stress. The energy released due to residual stress may lead to debonding of the coating at the interface. Dissolution of calcium phosphate coatings is determined by the degree of crystallinity i.e., more crystalline the calcium phosphate coating is, the lower its dissolution rate [31].

The reduction in thickness of coatings will overcome above mentioned disadvantages and therefore, study on different deposition technique to prepare Ca-P-O thin-films was carried out. Properties that govern good quality calcium phosphate thin-film include Ca/P ratio, surface roughness, hydrophilicity, crystallinity, biocompatibility and coating uniformity. In view of this Ca-P-O thin-films were deposited using two different deposition techniques, ion sputtering and atomic layer deposition (ALD). The main goals of this study were (i) preparation of transparent Ca-P-O thin-films for microscopic study of bone cells (ii) to obtain films with Ca/P ratio similar to natural HA (iii) to use low and high energy ion irradiation to improve the hydrophilicity of thin-films (iv) to understand the effect of surface roughness of titanium substrate and its influence to the atomic Ca/P ratio (vi) and to investigate the ALD Ca-P-O films on different surfaces as a cell culture substrate.

2 Thin films and titanium as biomaterials

This chapter presents an overview of Ca-P-O thin films and titanium metals used as biomaterials. The biocompatibility of a surface is a combination of many factors among which the correct surface chemistry, material mineral form and surface topography can be altered during the material or surface preparation.

2.1 Ca-P-O thin films

The use of Ca-P-O thin films is of interest, because of their similar chemical composition to that of apatite of living bone [1, 2]. Key characteristics which determine the durability of the coatings are optimal phase composition, a Ca/P atomic ratio approaching the stoichiometry ratio of HA, microstructure, low porosity, low internal stress, strong adhesion to the metal surface, chemical stability, crystallinity and surface roughness [32, 33]. Ca-P-O coatings used for implants must be non-toxic, biocompatible and cause no significant changes in the calcium phosphate levels [21] which improve the initial osseointegration rate [34]. This osseointegration process starts with gradual reabsorption of HA-like thin films, followed by direct contact of surrounding tissue with implant interface layer to form a strong attachment. In general Ca-P-O thin films have the potential to improve implant biocompatibility and ultimately implant longevity.

In order to achieve above requirement, thin Ca-P-O films have been prepared using different coating techniques. Continuous research on HA and Ca-P-O materials during the last few decades has not only focused on the tissue-coating interface, but also on the problems associated with the coating process and optimisation of coating properties for maximum tissue response.

2.2 Role of biomaterials in implantation

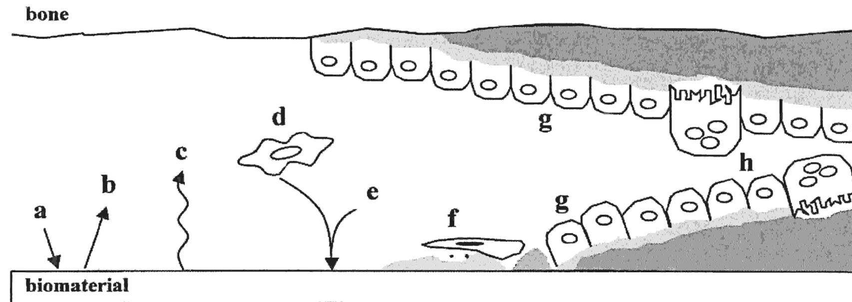

Figure 2.1: Representation of events at the bone-implant interface: (a) protein adsorbed from blood and tissue fluids, (b) protein desorption, (c) surface changes and material release, (d) inflammatory and connective tissue cells approach the implant, (e) possible targeted release of matrix proteins and selected adsorption of proteins, (f) formation of lamina limitants and adhesion of osteogenic cells, (g) bone deposition on both the exposed bone and implant surface, (h) remodeling of newly formed bone [35].

The concept of biomaterials is one that material elicits a specific biological response at the material-biosystem interface. In this present case, this results in the formation of a bonding zone between the tissue and material shown in previous study [20]. Though the mechanism behind the bonding zone still remains unknown. A possible prediction that might have led to this process is shown in the Fig. 2.1. This interface has been referred to as the bonding zone [21]. Though the development of this interface is complex and involves numerous processes, factors such as particle size, shape and surface roughness affects cellular adhesion, proliferation as well as phenotype plays an important role during bond formation. Cells can discriminate even the subtlest changes in topography and they are most obviously sensitive to chemistry, topography and surface energy [36]. A comparison between normal bone and HA structures shows a large similarity in both the channels and space required for bone cell ingrowth. This is a significant reason for the considerable interest in HA as a bone replacement [37].

2.2.1 Interface details

The dissolution characteristics of Ca-P-O thin films maybe critical for understanding tissue response to the coatings, a process which depends on chemical composition, crystallinity, porosity, particle size, surface area, as well as the ionic composition of the equilibrating solution (pH, ionic strength, concentration of the ion constituents) [38–40].

Material	Youngs Modulus /(GPa)	Yield Strength /(MPa)	Tensile Strength /(MPa)	Density /(gcm^{-3})
Ti	116	140–250	230–460	4.5
SS	190	209	519	7.8

Table 2.1: Physical properties of Ti and stainless steel (SS) [43–46].

The dissolution of thin films increases with an increase in porosity. The dissolution process is initiated with (1) partial dissolution of HA, releasing calcium and phosphorous ions, increasing their localised concentration in the microenvironment, (2) formation of precipitation on coatings, (3) ion exchange with surrounding tissue and (4) then the formation of a bone-like mineral layer [34]. The bone like mineral layer promotes the adhesion of the extracellular matrix, providing a preferential substrate for cell attachment.

Faster bone attachment was observed on thin films with a higher content of amorphous phase due to more rapid dissolution; however this may be lead to loss of fixation when compared to thin films with crystalline phase. Likewise a higher mineralised extracellular matrix has been reported to be formed on Ti coated with Ca-P-O thin films other than just the uncoated Ti implant [41].

2.3 Titanium as implant material

To overcome failures in load-bearing applications, mechanically poor Ca-P-O thin films can be combined with stronger metal implants. The implant metal used must form a stable interface with surrounding tissue and be in agreement with the mechanical properties of natural tissue. The metallic materials commonly used as implants are stainless steel (SS), cobalt chromium (Co-Cr) alloy, titanium (Ti) and its alloy Ti-6Al-4V, 6 wt.% Al, 4 wt.% V, $<$0.25 wt.% Fe and $<$0.2 wt.% O. Ti is mostly employed either in pure or alloy form because of its good corrosion resistance, reasonable fatigue life strength, comparatively high stiffness, light weight and relative inertness, as shown in Table 2.1. This table summarises the mechanical properties of Ti and stainless steel. An increase in bond strength between HA and Ti has been noted due to formation of chemical bonds between them in addition to the expected mechanical bond. Another important factor that has to be considered is the thermal expansion coefficient, where a difference between titanium (10.4×10^{-6} K^{-1}) and HA (13.4×10^{-6} K^{-1}) is observed [42]. Residual stress is minimised with a smaller difference in these coefficients. This is important because although the temperature change in the body is small, high temperature may be encountered during sterilisation process.

.

2.3.1 Modification of surface morphology

In the case of the adhesion between Ca-P-O coatings and metallic substrates, the surface nature of the substrate plays an important role. From previous studies it has been observed that a highly roughened surfaces exhibited better long-term clinical success with higher bond strength, greater resistance of the coating to pure shear forces and an increase in coating and body-fluid interface, when compared to a smooth substrate surface [47, 48].

Biological responses, at cellular level, such as migration of cells, orientation, osseointergation or tissue interaction with the surface of an implant not only depends on chemical composition but also on surface morphology [49]. Therefore, in order to control surface property of titanium substrate, an appropriate chemical and morphological treatment of the surface is necessary to achieve stronger bone-to-implant integration. The microstructure of implant surface can be modified using different techniques such as chemical etching, blasting, cutting, casting, rolling or mechanical polishing. In vivo tests of implants have shown that osteoblasts have higher probability to adhere to a rough titanium surface while fibroblasts and epithelial cells adhere mainly to very smooth surfaces [50,51]. Though rough surfaces promote the growth of the bone tissue over the implant surface, the optimum surface roughness is still not determined. The surface of a metal substrate can be classified smooth (microstructured), macrostructured or porous textured. The microstructured metal in terms of surface is altered either by acid etching [52, 53] or grit blasting [54, 55]. Grit-blasted, metal surfaces up to a roughness of four to ten μm R_{rms}, is typically used in preparation for application of a plasma-sprayed coating. Macrostructuring can take the form of grooves, threads, meshes or deposited metal coating.

3 Thin film deposition and modification

In order to obtain films of high optical quality for microscopic study in fixed- and live-cell imaging, the sputtering and ALD deposition methods were investigated. In addition we investigated ALD deposition on Ti as an approach for improving bone attachment on surgical prosthesis. Both the ALD and sputtering techniques have the advantage of being able to deposit optically transparent thin coatings with fairly high deposition rates. For sputtering even room temperature, deposition is possible. For selective surface modification without affecting the bulk properties, ion irradiation of the film at room temperature can be carried out. This modification can be considered in terms of: (1) cleaning and/or roughening of the surface, (2) changes in the surface composition and (3) the formation of hydrophilic and/or hydrophobic groups. This chapter gives a concise overview of experimental techniques and details used in this study. Fig. 3.1 gives the flowchart of sample preparation and experimental procedure carried in this study.

3.1 Sample preparation

3.1.1 Borosilicate and Si substrates

Before deposition, borosilicate glass coverslips and Si substrates, cut from the wafer were treated in hot acetone in an ultrasonic bath. Finally, the substrates were rinsed with isopropanol and blow dried with nitrogen gas.

3.1.2 Titanium substrate

In order to study the effect of roughness towards the growth of Ca-P-O thin films deposited using ALD, the surface topography of titanium substrates were modified. Commercial Ti plates 50 mm $\times$ 50 mm from Goodfellow [56] (purity 99.6+%) were cut to a size of 10 mm $\times$ 10 mm. The surfaces of the cut samples were subsequently treated using 600, 1200, 2000 SiC abrasive paper and 3 μm diamond paste (DP).

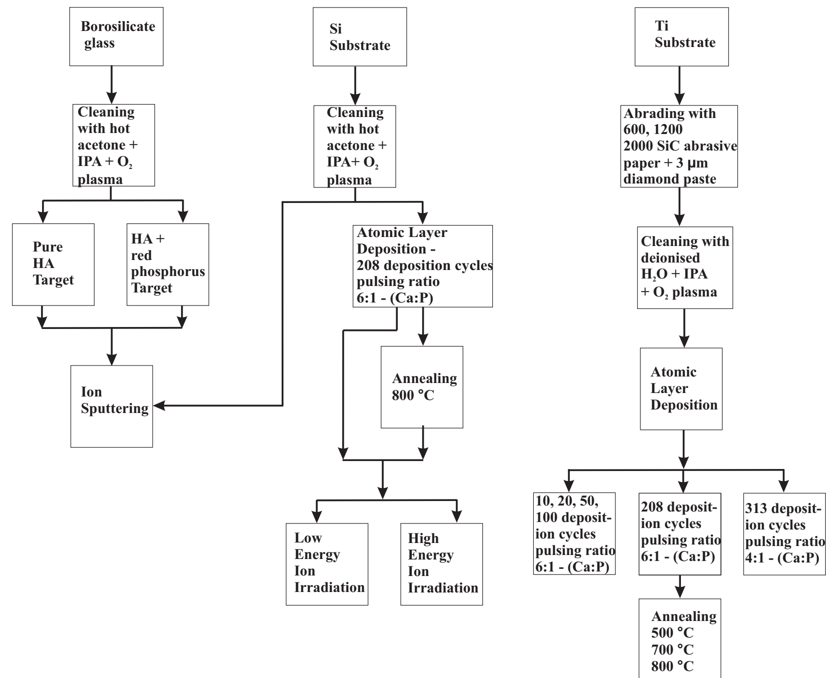

Figure 3.1: Flowchart of sample preparation for borosilicate, Si and Ti substrates.

The process was stopped at four different points. This yielded Ti substrate with four different surface roughnesses. Deionised water was used as a lubricating medium while abrading with SiC paper. Diamond paste polishing was done on clean room cleaning sheets. The treated samples were later ultrasonically agitated for 5 minutes in deionised water, isopropanol and finally blow-dried with N_2 gas.

3.2 Sputtering target preparation

In order to achieve a uniform thickness of Ca-P-O thin films, it is essential to optimise the deposition rate and measure the beam current. To obtain a Ca/P ratio similar to that of HA, two types of targets were prepared for this study; pure HA targets, made from commercially available HA powder [57] and composite mixture HA + red phosphorus targets, where the atomic percentage of phosphorous was increased from 13.6 at.%. for pure HA to 23.6, 33.6 and 43.6 at.%. The sputter targets were compacted from powder into disc-shaped pellets of 8 mm diameter and 2 mm thickness by 20 GPa uniaxial pressure.

3.3 Ca-P-O thin film deposition

Research on HA and calcium phosphate thin films has led to the use of different deposition techniques in order to optimise properties of coatings or thin films suitable for maximum tissue response. The most commonly used deposition techniques are plasma spraying, biomimetic coating, pulsed laser deposition and sputter deposition. This study focused on deposition by means of ion sputtering and ALD.

3.3.1 Ion sputtering

Sputtering is widely commercially used for the deposition of films, and also for anisotropic etching of structures in semiconductor industry and in micromaching technologies. A smooth and continuous coating is obtained by sputtering. Typically when an ion beam impinges a target, eroding the surface; most of the ion beam is implanted in the target to a depth depending on the energy of the ion beam used and a small fraction is reflected after suffering a range of energy losses. The slowing down of energetic ions in a target creates a so-called collision cascade. If the cascade of moving atoms extend to the surface, atoms that are outward directed may be ejected if they have enough energy to overcome the surface binding energy. The ejected target atoms which have a wide angular and energy distribution, can be collected on another surface, a collector (substrate) on which a deposited thin film is formed. This process is called *ion sputter deposition.*

In general when an incoming particle collides with the atoms of the solid, it transfers energy to the atomic nuclei. When more energy than binding energy is transfered a primary recoil atom is created. Primary recoil atoms collide with other target atoms creating a collision cascade. Thereby sputtering of surface atoms occurs if target atoms

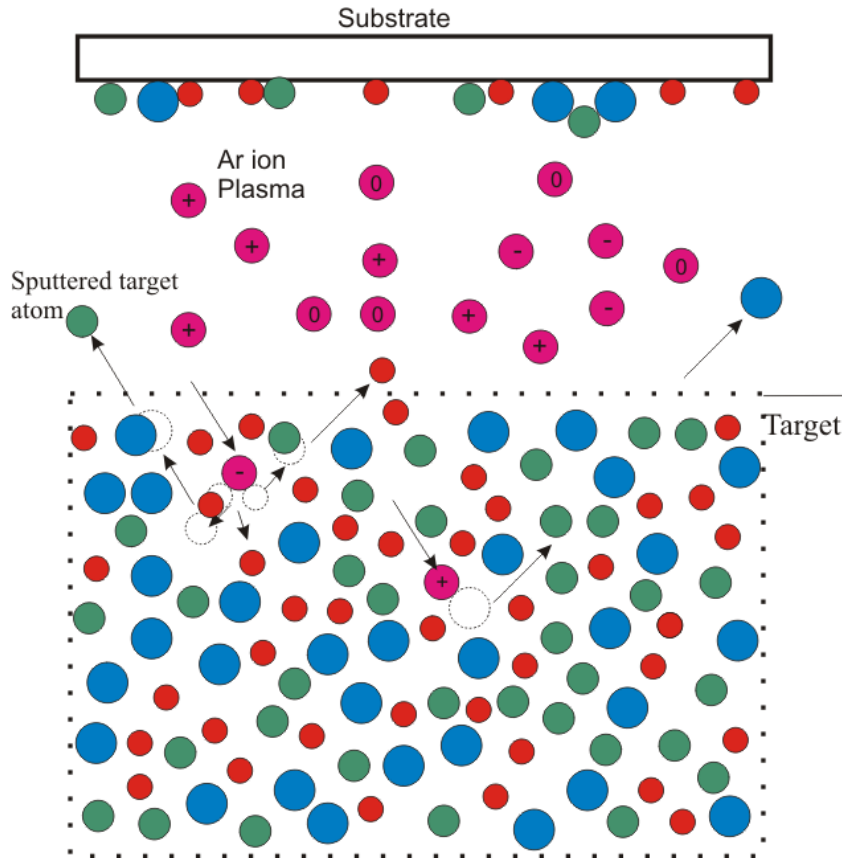

Figure 3.2: Sputter deposition of thin films with possible sputter mechanisms.

obtain enough kinetic energy to overcome the binding energy exerted by the target.

Fig. 3.2 illustrates the sputter ejection process. When an incoming particle collides with atoms of the solid, it is possible to characterise sputtering events to belong to one of the following types [58, 59]:
(i) Single knock-on region
(ii) Linear-collision cascades and
(iii) Non-linear cascacde (spike region)

Single knock-on region (low-energy light ions) is the region close to the sputtering threshold, where the energy to create full collision cascades is not available. However, for very light projectiles, a few collision events may take place at all energies. For target components with widely different masses and light projectile, preferential ejection of the lighter component of two component target will be favored. For the linear-collision cascade and spike region, the energy of imparted recoil atoms is greater and create secondary and higher-generation recoils of which few may approach the surface and overcome the surface energy barrier. In this case preferential sputter ejection is less

likely. In non-linear cascade the target atoms in the cascade are in motion prior to scattering atoms are ejected from a more or less well-defined thickness Δx_0 of a nm or so. The energy distribution of the sputtered atoms is peaked at 1–2 eV and has a long tail extending to higher energies.

The sputtering yield is expected to be proportional to the number of recoil atoms generated in that layer, and their kinetic energy which falls into lower and medium eV regions. According to Sigmund's theory [60] the sputtering yield in the linear cascade region can be expressed by:

$$Y = \frac{0.042\alpha(M_2/M_1)S_n(E, Z_1, Z_2)}{NU_o}. \tag{3.1}$$

Here, S_n is the nuclear-stopping force, α is an energy-independent function of the mass ratio between the target M_2 and projectile M_1 atoms. E is the projectile energy, (Z_1), (Z_2) are atomic number of projectile and target atom respectively. N and U_o are density and surface binding energy of the material. In the single knock-on region, the sputtering yield is given by the pertinent cross sections. For a linear cascade, it is proportional to the available energy, i.e., energy deposited per unit depth according to Eqn. 3.1. In the spike region temperature associated with the energy deposited is to be considered. Most ions in the tens of keV region give rise to a linear cascade. Higher energy and heavier ions (MeV ions) cause non-linear cascades.

From the point of view of thin film deposition the advantages of sputtering are (i) that refractory materials (oxides, nitrides, carbides and metal such as tungsten.) can be deposited. (ii) The greater than thermal energy of sputtered atoms promotes adhesion through ballistic atomic mixing at the film/substrate interface. (iii) The composition of the film is governed by the composition of the sputtered flux. Hence the composition of the deposited film can be constant throughout the thickness of the film. For our purpose sputtering was used to obtain optically transparent thin films which can be used for live-cell microscopic study. The major disadvantage of sputter deposition is the difference in Ca/P atomic ratio between the target and sputtered coatings due to the difference in partial sputtering yields y_{Ca} and y_P from a multi-component target and due to the preferential deposition of calcium. This is probably due to the possibility of the phosphorus ions being lost and pumped away before being prominently deposited at the substrate [34]. The difference can also be due to the collection efficiencies of Ca and P or loss of P from deposited films. It is also suggested that the phosphorus ions maybe weakly bound to the film being deposited and can be sputtered away by incoming low energy sputtered atoms [60–63]. The disadvantages of sputter deposition are the post deposition annealing needed to obtain crystalline film and dissolution of amorphous film in *in vivo*.

3.3.2 Sputter deposition at JYFL

The setup used for ion beam sputtering was constructed at Department of Physics, University of Jyväskylä and shown in Fig. 3.3 [64]. A tungsten filament was used to produce electrons to create a plasma from which stable ion beams from all gaseous elements could be extracted. The beam transport unit consists of an acceleration electrode, an Einzel-lens and extraction electrode. A sharply focused beam spot can be obtained by changing the potential of the Einzel-lens [64].

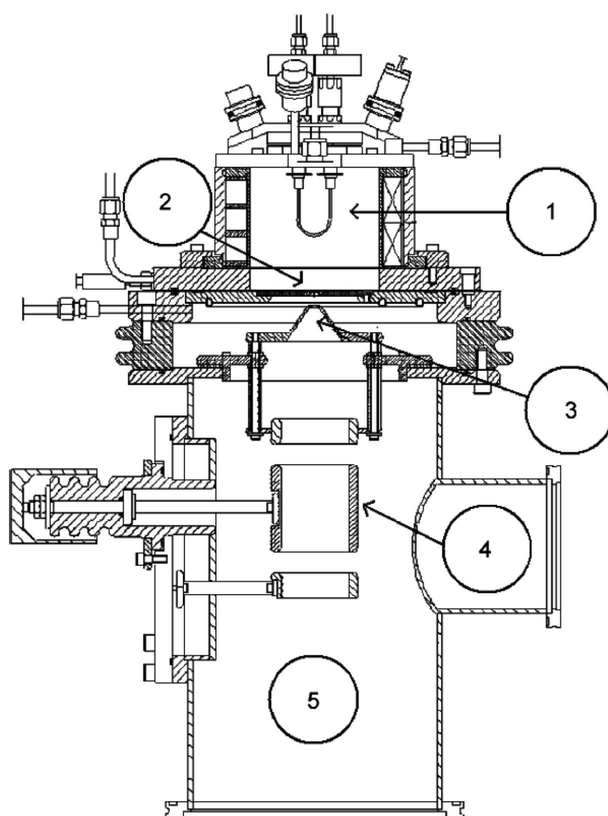

Figure 3.3: The sputtering instrument is shown in (a). It consists of (1) ion source, (2) plasma electrode, (3) extraction electrode, (4) Einzel-lens, and (5) sputtering chamber (With permission from [64]).

The beam is focused to the sputtering target by optimising the current in the target holder. The sputtering target HA pellet is embedded in a carbon holder and ion beam is impinged on the HA pellet at 45° to the surface normal. The substrate to be coated, was placed at 90° with respect to the incoming beam (Fig. 3.4).

The thin Ca-P-O coatings were sputter deposited on cleaned borosilicate glass and Si substrates at a chamber pressure of 10^{-6} mbar. Sputtering was carried out using N_2, Ar or Kr as the ion source feedstock gas at different acceleration voltages (2, 4, 6, 8 and 10 kV) with the same discharge current of 1.5 A. The ion beam impinged on the

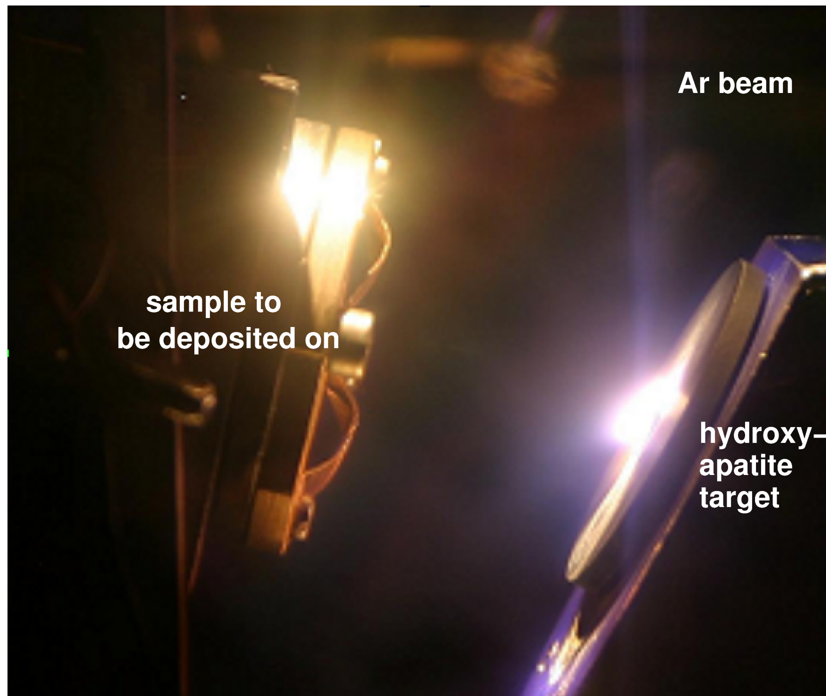

Figure 3.4: Deposition of hydroxyapatite films by means of an incident 6 keV Ar ion beam.

HA pellet and the sample target distance was fixed at about 3.5±0.5 cm. The films were deposited up to a thickness of about 100 nm with a maximum deposition rate of 0.7 nm s^{-1}.

3.3.3 Atomic layer deposition

Atomic Layer Deposition is a widely expanding technique belonging to the group of chemical vapor deposition methods (CVD) [65, 66]. In traditional CVD the film growth occurs due to a decomposition reaction of constantly flowing gaseous precursors. Whereas in the ALD deposition process it runs below the decomposition temperature of precursors. The substrate is exposed only to one precursor at a time in order to avoid the reaction between the precursors thereby maintaining the quality of the thin film. ALD is thus a single atomic layer by layer process where the film is built up by reaction at the surface from pulses of precursor gas. A schematic representation of ALD process is shown in the Fig. 3.5.

The film growth reaction occurs between the precursor vapor and one monolayer of the other absorbed precursor on the substrate. After all the reactive groups are consumed with no further reactions, the surface is covered with monolayer of the second precursor. Inert gas, such as N_2, is typically used to purge out excess precursor. The cycle of

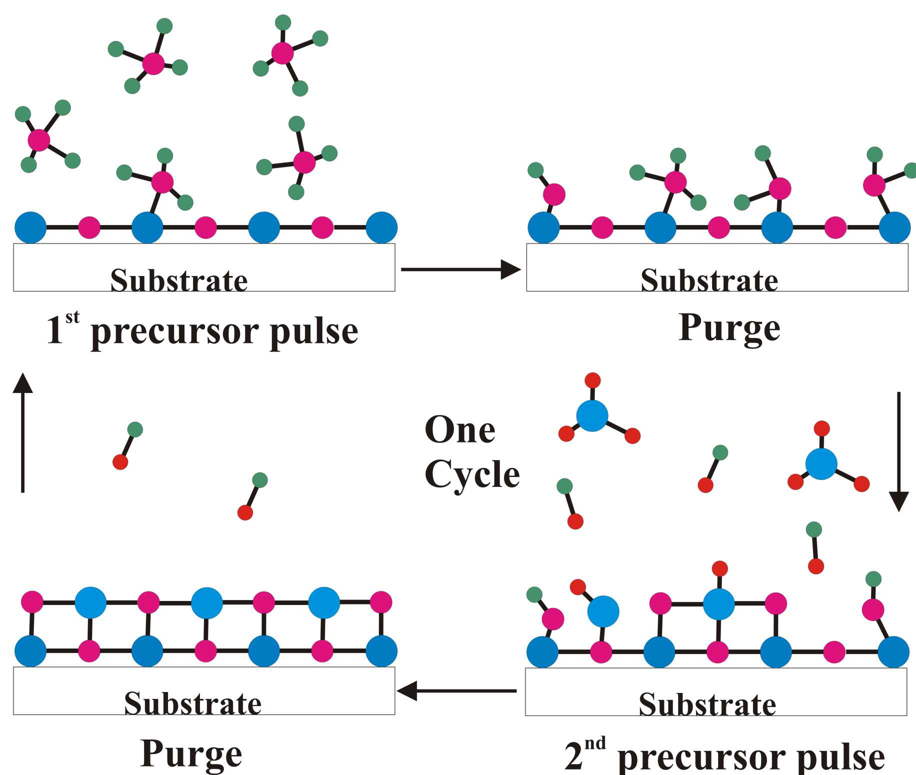

Figure 3.5: A schematic representation of ALD process.

first precursor, purge, second precursor, purge is then repeated to deposit subsequent layers. Since the film growth reaction are obtained after saturation of chemical process, the deposited films are highly conformal and pinhole free. Two main requirement for ALD deposition are highly reactive precursors and growth temperatures below the self-decomposition temperature in order to obtain impurity free and self-limiting saturated film growth. The film thickness obtained by this process is uniform through out the substrate. Thickness is governed by the the number of deposition cycles. A highly uniform film with thickness down to the nanometer range defined stoichiometry values can be produced. Another major advantage is that because the reactant precursors are delivered in a gas phase, ALD can be used for coating three dimensional structures with intricate shapes and features [67].

ALD was used in the initial phase of this study [68] to deposit Ca-P-O films. The as-deposited films were amorphous in nature. Formation of crystalline phases typical of hydroxyapatite were observed to form at 500 °C according to X-ray diffraction studies [68]. The degree of crystallinity increased at higher annealing temperatures.

3.3.4 Ca-P-O Parameters for ALD deposition

Ca-P-O films were deposited on Si and Ti substrates using an commercial ASM F-120 flow-type ALD reactor. $Ca(thd)_2$ (thd = 2,2,6,6–tetramethyl–3,5–heptanedione) and trimethylphosphate ($(CH_3O)_3PO$) were used as calcium and phosphorous precursors, respectively. Amorphous surface-controlled Ca-P-O thin films were deposited at 300 °C. The $Ca(thd)_2$ and trimethylphosphate precursors were evaporated by means of their own vapor pressure from open glass boats placed inside the ALD system at 190 °C and 25 °C, respectively. Ozone and deionised water were used as oxygen sources after the $Ca(thd)_2$ and trimethylphosphate pulses, respectively. Water was evaporated by means of its own vapor pressure from an external container at 25 °C. Ozone was generated from 99.999% oxygen with a Fischer 502 ozone generator. Nitrogen (99.999%) was used as a carrier and purge gas, which was generated from dry compressed air with a Schmidlin UHPN 3000 nitrogen generator.

The growth mechanism of ternary Ca-P-O proceeded by a two-step fashion producing first calcium carbonate and then successive $(Ch_3O)_3PO/H_2O$ cycles subsequently convert some of the carbonate to phosphate. A Ca-P-O ALD cycle consists of Ca and P subcycles. The ratio of subcycles were adjusted to obtain the desired Ca/P molar ratio in the film. A typical deposition cycle aiming at a stoichiometric Ca:P molar ratio of 1.67 consists of a Ca subcycle repeated 6 times followed by one P subcycle. Prior to the thin film deposition the Ti substrates were cleaned using O_2 plasma etching. ALD films of 10, 20, 50, 100 and 208 cycles were deposited on Ti and on Si samples. A The as-deposited thin-films were annealed after deposition in an ATV PEO 601 rapid thermal annealing oven under humid argon (99.999%) atmosphere at 500–800 °C for 10 minutes to obtain the desired crystalline hydroxyapatite phase. The film thickness for a sample deposited with 208 ALD cycles is between 50 and 60 nm.

3.4 Ion interaction with materials

In this work we aimed to alter the surface properties of a thin films of Ca-P-O in order to enhance their biocompatibility while retaining the bulk properties of the film. Both low and high energy (keV and MeV) ion irradiation can alter the surface and bulk film properties such as crystallinity [69], wettability [70, 71] conductivity [72] and solubility [73].

There are three major classes of the energetic ion interactions with materials. These are: (i) Electronic excitations and ionisation events - these happen at all ion energies. They result in break of chemical bonds, new molecule formation, secondary electron emission, electron-hole pair generation, luminescence, intrinsic defect production,

change of valence state of impurities, sputtering and radiation emission. (ii) Atomic collisions (direct momentum transfer from the incident ion to the target atom) are the most significant mainly at low energies and include sputtering, molecule formation or decomposition, atomic mixing and intrinsic defect production. (iii) Doping (implantation process) – foreign atoms are introduced in the target and at high fluences can result in compound formation within the target.

When an energetic ion traverses through matter it interacts with nuclei and electrons of the target through collisions, before coming to rest [74]. One of the most important quantities associated with this slowing down process is the stopping $\mathrm{d}E/\mathrm{d}x$, which is the average energy loss $\mathrm{d}E$ of the incoming ion per unit elemental path length $\mathrm{d}x$. This is the *stopping force* of matter for an ion [74–76]. The ion transfers its kinetic energy to the medium by two main processes, *nuclear stopping* and *electronic stopping*.

The total stopping force, $\mathrm{d}E/\mathrm{d}x|_{tot}$, can than simply be expressed by,

$$\frac{\mathrm{d}E}{\mathrm{d}x}|_{tot} = \frac{\mathrm{d}E}{\mathrm{d}x}|_{n} + \frac{\mathrm{d}E}{\mathrm{d}x}|_{e}, \tag{3.2}$$

where subscripts n and e refer the total nuclear and electronic stopping, respectively. Typical energy losses are of the order of a few to many 100 eV/nm depending on the, ion, its energy and target composition [75].

In a nuclear collision at keV energies, an energetic ion transfers some of its kinetic energy to a target atom by scattering in a screened coulomb interaction. The collision can be considered to be a binary collision, (i.e a two body collision) since the energy transfered is large compared to binding energies [75] and the electrons only contribute electronic screening of the nuclear charges. The nuclear stopping or nuclear energy loss is an elastic collision process. This process is predominant when the incident ion has low energy E_0 and high atomic number Z_1 [74, 75].

In electronic stopping, the ion's energy is transferred to the electrons of the target atom by two main mechanisms; electronic excitation and ionisation through a coulomb interaction. It should be emphasised that both excitation of the projectile and target atoms contribute to stopping. The electronic stopping mechanism is essentially an inelastic process; which is dominant when the ion has high energy, E_0 and low atomic number, Z_1 [77].

3.5 High energy irradiation

3.5.1 Tandem Pelletron accelerator

To study the effect of high energy irradiation and for analysis the 1.7 MeV tandem Pelletron accelerator (National Electrostatic Corporation, USA) in Jyväskylä was used. This accelerator is equipped with an RF ion source (Alphatross) which generates negative ions of H, He and O. These negative ions are preaccelerated to few tens of keV energy, E_i, and mass-energy filtered by Wien velocity selector[1] and subsequently focused by an Einzel lens before injected into the accelerator. The negative charged ions are accelerated towards the high voltage terminal in the center of accelerator tank by the attractive force from the positively charged terminal. Inside the terminal they pass through a stripper filled with low pressure N_2 gas. In collisions with N_2 molecules the negative ions are stripped of electrons rendering them positively charged. These positive ions are then accelerated by the positively charged terminal in the second acceleration stage towards the ground potential. The total kinetic energy acquired by the ion is therefore $E = (1 + q)\,V + \mathrm{E}_i$, where V is the terminal voltage in MV, q is the charge state of the positive ion. Protons can therefore be accelerated to $E = 2\,V + \mathrm{E}_i$. Other ions may create several charge states after they pass through the stripper, e.g. $^{16}O^-$ can form ^{16}O, $^{16}O^+$, $^{16}O^{2+}$, $^{16}O^{3+}$, etc with progressively higher charge states. The desired charge state with corresponding energy is selected by a switching magnet and directed into the lithography beam line (-15°).

3.5.2 Programmable Proximity Aperture Lithography

A high energy ion beam was used to lithographically irradiate the thin films using the PPAL system in which, heavy ions beams can be shaped to small rectangular beam spots. The aperture in the PPAL system is made up of four 100 μm thick, well polished edges of Ta foils [78, 79]. Two foils are glued together with a vacuum compatible epoxy adhesive, Torrseal^{TM} at right angles to form a L-shaped blade [78, 79]. Each L-shaped blade is glued to a corresponding Al block which is mounted on a high precision positioner (Fig. 3.6(b)). By moving the blocks in X' and Y' direction a precise rectangular aperture opening can be defined. The sample holder is mounted on three similar positioners which can move the sample in the x, y and z directions as shown in Fig. 3.6. Combining the X',Y', x and y movements allows complex patterns made up of rectangle pattern elements can be written.

A fluorescent screen on one of the aluminum blocks that support the aperture L-

[1] This has since been replaced with a inflection magnet.

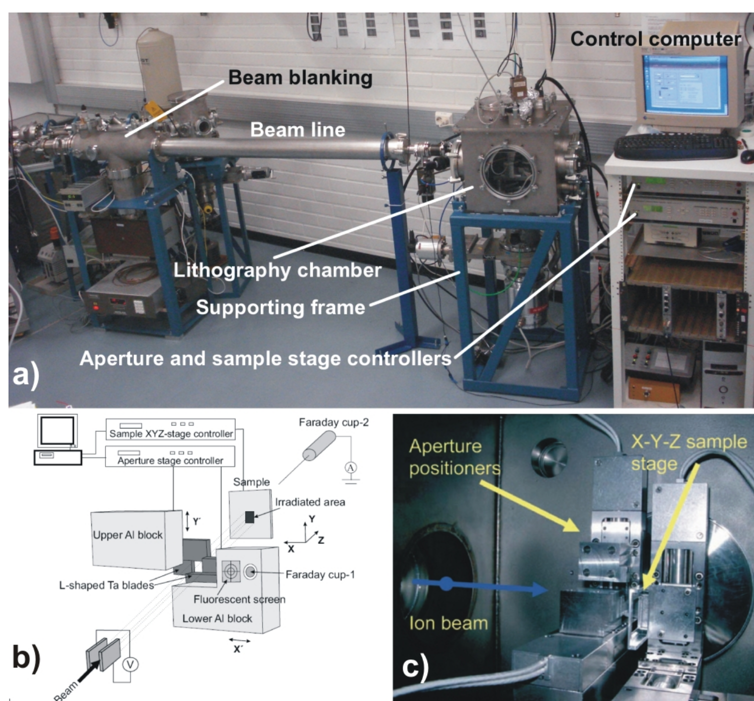

Figure 3.6: The PPAL system. a) The PPAL system at Pelletron laboratory. b) Schematic presentation of the operational principle of the PPAL system. c) A photograph of the interiors of the PPAL chamber. The Al block are mounted on high precision computer-controlled linear-motion drives that move the L-shaped Ta blades [80].

blades is used for optimising and focusing the beam to few mm in diameter. Purpose-developed LabVIEW^{TM}-based software is used to control the motion of the positioners, beam blanking and perform automated exposures by reading a sequential ASCII file containing pattern information [81].

3.5.3 Irradiation parameters

Both as-deposited and annealed Ca-P-O thin films were irradiated utilising the PPAL setup. The required fluence *(ions/cm^2)* per pattern element is then calculated from measurement of beam current density. The beam current density was determined from the Faraday cup. The high energy irradiation was carried out with a 2 MeV $^{16}O^+$ beam from the Jyväskylä 1.7 MV Pelletron accelerator. Exposures of square areas of 500 μm side length with 500 μm pitch were repeated to cover a 5 mm$\times$5 mm area. The fluence of 10^{14} ions cm^{-2} was obtained with 500 pA beam current through the aperture. Irradiation was carried out at a pressure of 10^{-6} mbar.

3.6 Low energy irradiation

3.6.1 Ion irradiation system

Low energy electron bombardment can produce recrystallisation of amorphous pockets [82–85]. In order investigate the effect of ion irradiation on as-deposited and annealed ALD deposited HA films, low energy ion irradiation was carried out using an Electron Cyclotron Resonance (ECR) plasma source.

The magnetic field in ECR ion source consists of an axial component which is generated by solenoids or permanent magnets and a radial component which is usually multipole field produced by permanent magnets. The orbital electron motion allows the electron to collide with many atoms and ionise them to form a dense and hot plasmas. Higher magnetic field gives higher frequency which leads to higher plasma densities and consequently higher extended ion beam intensities [86].

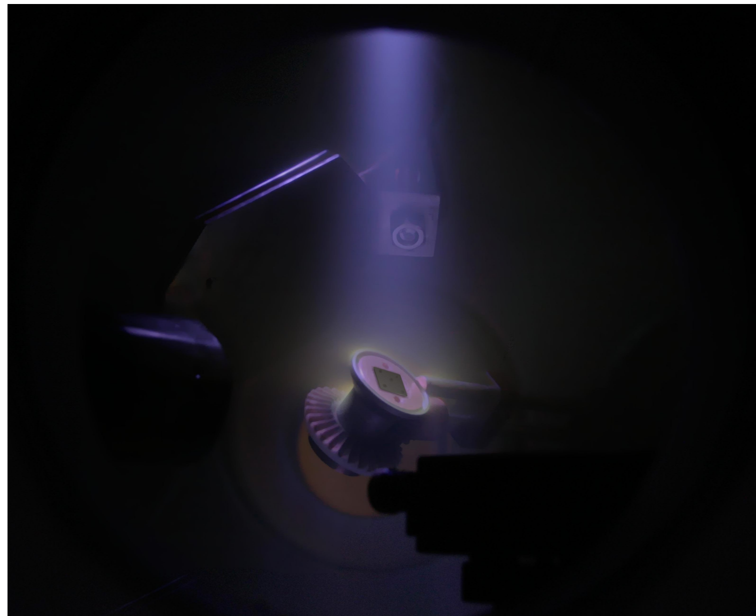

Figure 3.7: Irradiation of a Ca-P-O film by means of Ar ion beam.

3.6.2 Irradiation parameters

Both as-deposited and annealed Ca-P-O thin films were irradiated with low energy ion beam from OSPrey Microwave Plasma Source from Oxford Scientific. Ar was used as the ion source gas feedstock for irradiation and the acceleration voltage was varied in steps from 0.6 kV to 1.2 kV ions for 90 s with the fluence of 4.5×10^{16} ions cm^{-2} (assuming +1 ion charge-state). The non-analysed beam from the source was anticipated to be a mixture of neutral Ar and low positive charge state Ar ions. The samples of 10 mm$\times$10 mm in size were placed in the sputtering chamber and evacuated to a base pressure of 1×10^{-6} mbar. The chamber pressure was then raised to 4×10^{-4} mbar with Ar feedstock gas. Once the processing pressure was reached, the source was turned on and the samples were irradiated at the respective acceleration voltage. To provide an un-irradiated control area on each sample, a 10 mm $\times$ 5 mm Ta sheet aperture mask was used to shield part of the sample surface from the ion beam. Fig. 3.7 shows the irradiation process.

4 Sample characterisation

The quality of Ca-P-O thin films which were produced and modified was determined by characterising the film composition, the hydrophilicity of modified surfaces, surface topography and MC3T3 mouse osteoblast cell culture studies on thin films. This chapter gives a brief overview of analytical methods that were utilised. Fig. 4.1 gives the flowchart of the different characterisation done with respect Ca-P-O films deposited on borosilicate glass, Si substrate, abraded Ti substrates deposited using ion beam sputtering and ALD, respectively.

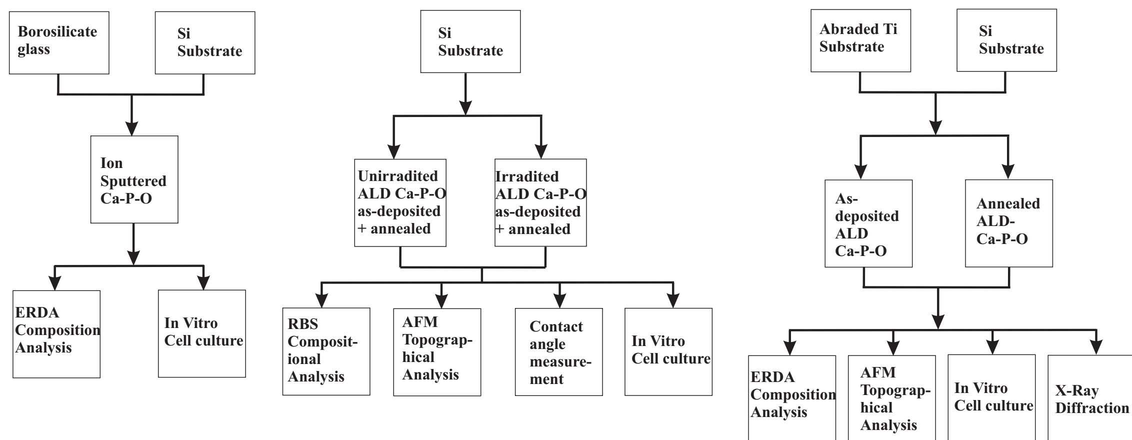

Figure 4.1: Flowchart of Ca-P-O thin film characterisation deposited on borosilicate, Si and abraded Ti substrates.

4.1 Rutherford Backscattering Spectrometry

Rutherford Backscattering Spectrometry (RBS) is an ion scattering technique that is used for compositional analysis of thin films. A sample target is typically bombarded with He ions at an energy in the MeV-range (typically 0.5–3 MeV) and the energy of the backscattered projectiles is recorded with an energy sensitive detector, usually a solid state ion implanted, surface barrier or p-i-n detector. The depth in which the scattering occurred can be calculated by means of scattering kinematics and the stopping force. If different elements in the sample are homogeneously distributed and detected without overlapping signals E=*(dE/dx)*, like in the case of Ca and P on Si, atomic ratios can be calculated by means of scattering cross sections for each element. It is also possible to obtain quantitative depth profiles from the RBS spectra (for thin films that are less than 1–5 μm thick). Moreover, the stopping cross-sections of many materials for most commonly used hydrogen and helium ions are experimentally well known. RBS is quantitative without the need for reference samples, fairly nondestructive and has a good depth resolution of 25 nm FWHM and 5 nm in some cases (e.g. for glancing incidence [87]. The major drawback of RBS is its limited sensitivity to detect light elements in a heavier matrix such as measuring thin films on heavier substrates. Because of this limitation, RBS could not be used for precise measurement Ca/P atomic ratios on Ti susbtrate in this study.

4.1.1 RBS measurements

The composition of the irradiated films on borosilicate glass and Si was determined with a 2 MeV $^{4}He^{+}$ ion beam backscattered at 160°. The 2 mm diameter beam was incident at 7° to the sample surface normal in order to minimise channeling. The SIMNRA simulation program was used to obtain the elemental Ca/P atomic ratio by comparison of simulated and experimental RBS spectra.

4.2 Elastic Recoil Detection Analysis

Elastic Recoil Detection Analysis (ERDA) is a powerful technique for quantitative depth profiling of all the elements in a sample. In ERDA, the sample to be analysed is mounted at a glancing angle with respect to an impinging ion beam. The projectile ion causes target atoms to be recoiled in forward directions by a single high energy collision, and these recoils are detected in ERDA together with scattered projectiles. The energy distributions of the different atoms ejected from the target at a given angle are measured, and can be, by means of known scattering kinematics, scattering

cross-sections and stopping forces, converted to elemental depth profiles [88]. Time of Flight–Elastic Recoil Detection Analysis (TOF–ERDA) is based on the simultaneous measurement of both the velocity and total energy of the atoms recoiled from the target to distinguish recoils of different elements. The velocity is determined from two independent timing detectors and the energy from a charged particle detector. In TOF–ERDA, normally beams of heavy ions like Cl, Cu, Br or I are used. Using the recoil atom velocity and energy, the isotropic mass of the particle can be calculated [89]. The depth profiles are obtained from the energy loss, as the ions travel into and exit from the sample surface [88]. The advantage of using TOF–ERDA in this study is that all elements in the sample, including hydrogen, can be well resolved and simultaneously detected (≤ 1 μm film thickness).

4.2.1 TOF–ERDA measurements

The TOF-ERDA measurements in this study were either done at IMEC, Belgium or in Jyväskylä. The elemental composition of sputtered Ca-P-O film on glass was measured at IMEC [90] using a 16 MeV $^{63}Cu^{7+}$ ion beam was directed to the sample and the TOF and the energy of recoiled sample atoms was measured at 38° with respect to the beam direction.

At the Jyväskylä Accelerator Laboratory depth profiles of the samples were measured with a recently constructed TOF-ERDA spectrometer shown in Fig. 4.2. It is installed in one of the beam lines of the 1.7 MV Pelletron accelerator. The energy dependent detection efficiency of the TOF detector for H is 35-65% for the energy range used in this study. The detection efficiency for carbon and heavier recoil is greater than 99.5% [91].

In the measurements on Ti substrates a 11.9 MeV $^{63}Cu^{6+}$ ion beam impinges on to the sample and the time of flight (velocity) and energy of recoiled sample atoms are measured with a detector telescope at 41° angle with respect to the beam direction. The Ca/P atomic ratios of the thin-films were calculated from the total recoil yield for Ca and P using scattering cross sections in order to minimise the influence of the uncertainties in the predicted stopping force. In the case of rough Ti films, the surface roughness broadening effects [92] are clearly visible, but care was taken in order to produce comparable results for samples with different roughnesses.

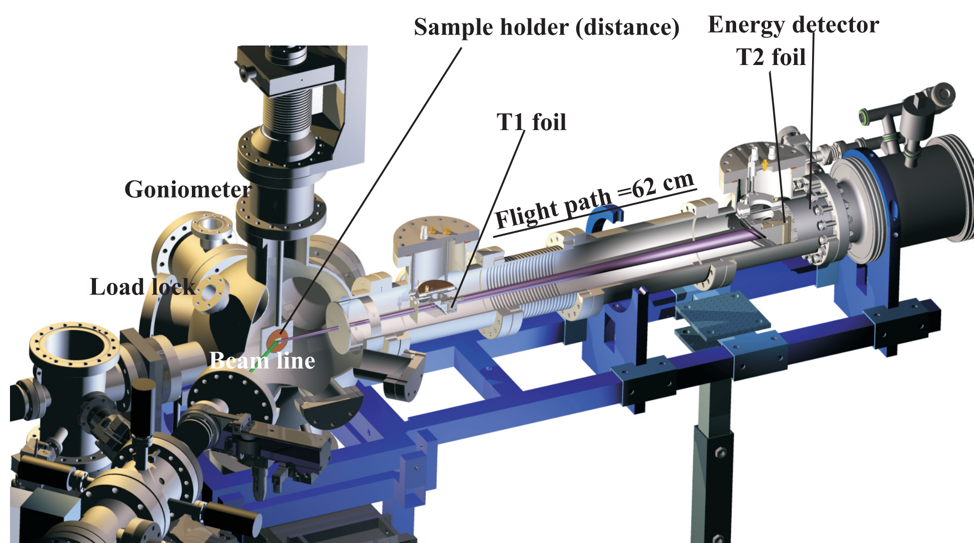

Figure 4.2: TOF-ERDA experimental set-up at at Jyväskylä Accelerator Laboratory. (Image courtesy of Mikko Laitinen).

4.3 Atomic Force Microscopy

Scanning probe microscopes (SPM) define a broad group of instruments used to image and measure properties of material, chemical and biological surfaces. The atomic force microscope is essentially a combination of the scanning tunneling microscope and the stylus profilometer. Atomic force microscopy (AFM) is based on sensing the force between a sharp tip (less than 50 nm in radius) and surface of interest (area less than 100 μm$\times$100 μm). It can be used to investigate both conductors and insulators on an atomic scale. Interpretation of AFM images depends critically on the details of the tip-sample interaction, which is via a single atom at very the end of the tip [93].

The three modes of operation of AFM which are widely used are contact mode, non-contact mode and tapping mode.

In *contact mode* an AFM tip makes soft physical contact with the surface and operates by rastering a sharp tip (made either of silicon or Si_3N_4 attached to a low spring constant, 10^{-9} Nm, cantilever) across the sample. The contact force (short-range interatomic forces) causes the cantilever to bend in order to accommodate changes in topography. Contact mode is typically used for scanning hard samples [93].

Non–contact mode: By moving the tip away from the sample to 10-100 nm, longer range forces, such as magnetic, electrostatic and attractive van der Waals forces, become successible. Instead of measuring static cantilever deflection, as in contact mode atomic force microscopy, the cantilever is driven to vibrate above its resonant frequency by a small piezoelectric element and the variation in driving force is measured [93].

Sample destruction during contact mode AFM, has been addressed through the development of tapping mode AFM. In *tapping mode*, The AFM tip-cantilever assembly oscillates above the sample surface while the tip is scanned; thus the tip lightly taps the sample surface while rastering and only touches the sample at the bottom of each oscillation. This prevents damage to soft specimens. By using a constant oscillation amplitude, a constant tip-sample distance is maintained until the scan is complete. Tapping mode AFM has the advantage, that it can be performed on both wet and dry sample surfaces [93].

One of the great advantages of the AFM is the ability to measure the sample surface in X,Y and Z dimensions thus enabling the presentation of three-dimensional images of a sample surface. AFM neither requires a vacuum environment nor any special sample preparation and it can be used in either an ambient or liquid environment [93].

4.3.1 AFM measurement details

In order to characterise the topography of irradiated films, tapping mode atomic force microscope (Digital Instruments, Dimension 3100, Veeco Metrology Group) measurements were made using a cantilever with a tip radius less than 10 nm [94]. The R_{rms} value for roughness was determined from three random 75 μm $\times$ 75 μm scans from different area of the sample in order to get a representative value.

4.4 X-ray diffraction

In order to determine the crystalline phase formed on annealed Si and Ti substrates the variable temperature X-ray diffraction (VT-XRD) was used. XRD is suited for characterisation and identification of crystalline phases. Other information obtained can include the degree of crystallinity present and grain size. In VT-XRD, X-ray diffraction is combined with thermal annealing, which records crystalline phase information on the material while it is subjected to a series of temperature changes [95]. VT-XRD can provide valuable information with regard to phase transitions, crystal structure, melting, decomposition, and crystallisation thin films.

4.5 X-ray diffraction measurement details

VT-XRD data were recorded with PANalytical X'Pert PRO diffractometer in Bragg-Brentano geometry using step-scan technique and beta-filter to produce Cu Kα radiation (1.54184 Å; 45 kV, 35 mA). The as-deposited Ca-P-O films on Si and Ti substrates were placed into a Anton Paar XRK900 high-temperature reaction chamber equipped with automated sample-stage height-controller. A moist argon atmosphere was generated by passing argon flow (60 ml/min) through a H_2O saturator prior entering into the chamber. The samples were heated to the desired temperature with a heating rate of 20 °C/min. At least two consecutive data acquisitions were made at each temperature (25, 400, 500, 600, 650, 700, 750, 800 °C) using continuous scanning mode in 2 range of 18–55 ° with a step size of 0.017 ° and counting times of 60 seconds per step (total time of 18 min/acquisition). Programmable divergence slit (PDS) was used in an automatic mode to define the irradiated length on a sample to 8 mm together with fixed 10 mm incident beam mask to form constant 80 mm^2 exposure area on a sample. The data processing and the search-match phase identification analyses were carried out using X'Pert HighScore Plus v.2.2d software with ICDD PDF-2 powder diffraction database implemented in Highscore Plus.

4.6 Surface wettability

Surfaces are critical in biomaterials and the properties of an implant surface, such as wettability, chemical composition, electric charge, surface roughness, porosity, etc., play a critical role in the adhesion processes of cells. Control of the hydrophilic or hydrophobic nature of the surface is particularly important [96, 97] in artificial biomaterials, some application microelectronics and thin film coatings.

The hydrophilicity of a surface can be characterised by the wettability. Wettability or wetting is the actual process where by a liquid spreads on a solid substrate or material. Wettability can be estimated by determining the contact angle or calculating the spreading coefficient. Wetting or spreading of a liquid on a solid surface or material depends on the solid surface properties as well as the liquid used.

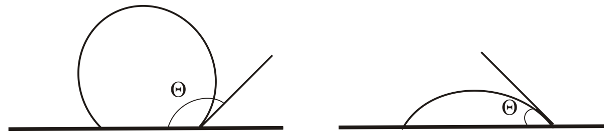

Figure 4.3: A liquid droplet in equilibrium with a horizontal surface. To the left: A non-wetting fluid with $90°\leq\theta\leq180°$. To the right: A wetting fluid with $0°\leq\theta\leq90°$.

Depending on the type of surface and liquid, the droplet may take a variety of shapes as illustrated in Fig. 4.3. The wetting angle θ is given by the angle between the interface of the droplet and the horizontal surface. The liquid is deemed wetting when $0° \leq \theta \leq 90°$ and non-wetting when $90° \leq \theta \leq 180°$. θ=0 degrees corresponds to perfect wetting and the drop spreads forming a film on the surface [98].

4.6.1 Contact angle measurements

Wettability measurements were carried out immediately after the irradiation. The wetting property of the surface was determined by measuring from a digital image the height of a sessile water droplet, as shown in Fig. 4.4, *(Y)* as a function of distance *(x)* from its left edge using a in–house software tailored to this purpose [99]. Smoothing of the boundary between droplet surface and the background was realised by fitting of *Y(x)* with a suitable functional form (sphere or ellipse), after which the angle between *Y(x)* and the substrate was obtained. This contact angle was determined at room temperature for both deionised water and cell culture medium, which contains α–MEM [100], fetal bovine serum, penicillium, streptomycin and L–glutamin. Typically, the volume of the drop used was about 10 μl.

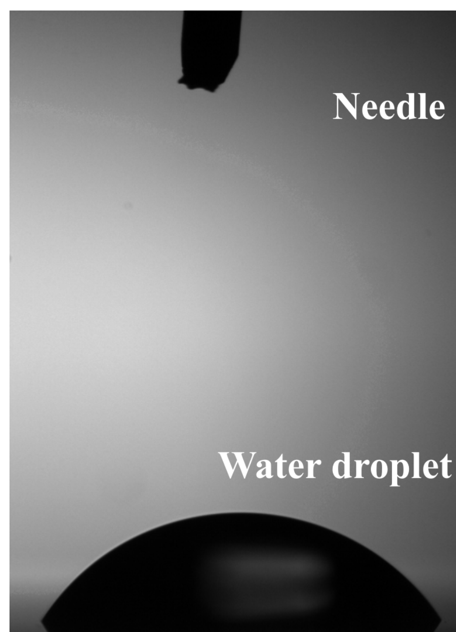

Figure 4.4: Water droplet dropped from the needle on the surface of Si substrate.

4.7 In vitro cell studies

For a material to be biocompatible depends on the living environment and it must not introduce any detrimental changes. Debris effects could lead to toxicity and induction of immune system responses. A complete biocompatibility test would involve cell culture with other bone cell types such as osteoclast and osteocytes and animal tests. In order to gain a complete insight into the biological performance of deposited Ca-P-O films, *in vitro* studies have to be performed. This study is restricted to testing the actual thin film responses of pre-osteoblast cells to the physiological environment. The *in vitro* biological properties of Ca-P-O thin films on Si and Ti substrate were evaluated by investigating cell morphology and proliferation, providing important base information about biocompatibility. Thus these Ca-P-O deposited films on Si and Ti substrates were treated as cell culture substrates.

4.7.1 Cell culture experiments

To investigate the biocompatibility of the films newborn mouse calvaria-derived MC3T3-E1 pre-osteoblastic cells (ATCC) were cultured in alpha-MEM medium (Gibco-Invitrogen) supplemented with 10% fetal bovine serum (Gibco-Invitrogen, USA), 100 U/ml penicillin, and 100μg/ml streptomycin (Gibco-Invitrogen) [101] at 37 °C in an atmosphere with 100% humidity and 5% CO_2. The complete medium was replaced every 2 days

and 70% confluent cells were sub-cultured through trypsinisation. The films were sterilised twice in 70% ethanol for 30 min and washed 3 times by $1\times$ phosphate buffer saline in the 24-well culture plate. To investigate the biocompatibilty of the films, cells at passenger 3 were harvested and seeded at a density of 1×10^4 cells/well on the films within 24-well plates. After 24-hour, 48-hour attachment and proliferation, the samples were washed with $1\times$ phosphate buffer saline and fixed with 4% paraformaldehyde for 15 minutes at room temperature. The actin cytoskeleton was stained with Alexa 488 labeled phalloidin (Molecular Probes, USA) and the nuclei was stained with Hoechst 33258 (Sigma). The samples were embedded into Mowiol including 2.5% DABCO. The cells were visualised by using an Olympus BX 50 epifluorescence microscope with ColorViewIII camera both from Soft Imaging Systems and AnalySIS 5.0 software. The images were further processed with ImageJ software [102].

5 Experimental results and discussion

In this chapter, the results and discussion of the experiments carried out during the course of work are described. The motivation for studying different deposition methods is to find a technique to obtain Ca-P-O films with composition close to that of stoichiometric hydroxyapatite and to set a growth substrate for osteoblast cell studies. Results from all studies are briefly summarised here.

5.1 Composition of Ca-P-O thin film

5.1.1 Atomic layer and sputter deposited films

The composition of thin films in this thesis was studied by means of two ion beam analysis techniques, TOF-ERDA and RBS. TOF-ERDA measurements were performed both at IMEC in Belgium and in Jyväskylä. The RBS studies were done in Jyväskylä.

As two very different techniques - one physical and one chemical vapor deposition technique - were used to deposit Ca-P-O films, it was not surprising that film compositions also were different. Fig. 5.1 (a) shows the energy histogram and corresponding elemental depth profiles of Ca-P-O thin films deposited using ion beam sputtering. The film thickness was about 100 nm. The thin film sputtered using argon showed greater number of impurity elements such as carbon, nitrogen, sodium and aluminum. The origin of excess hydrogen is most likely residual water in the sputtering chamber and target. High carbon content in the film can be associated with a misaligned beam hitting the carbon mounting during the deposition process. The origin of Na and Al remained unclear. A Ca/P atomic ratio of 1.6 approaching the stoichiometric ratio of HA was obtained for the film sputtered using Ar as feedstock at 10 kV from a HA+red phosphorus target corresponding to 43.6 at.% P. On the other hand the films sputtered from pure HA targets and targets with lower P content showed Ca/P ratios greater than 2. Similar results have earlier been reported for RF sputtered films which were deposited using pure HA target [103, 104].

The TOF-energy histogram and corresponding depth profiles of a thin film deposited

using ALD are shown in Fig. 5.1(b). ALD films generally had lower impurity content. A Ca/P of ratio of 1.64 was obtained for as-deposited 50 nm thick film. Whereas non-stoichiometric Ca/P atomic ratio was obtained for annealed Ca-P-O film on Si substrates (Fig. 5.2) due to loss of phosphorous during annealing. When the film composition was studied as a function of ALD cycles, it was found that the Ca/P ratio increases with the number of cycles (Fig. 5.3), and thinnest films are very P-rich.

When these two deposition techniques are compared, the sputter deposition has the great advantage of being a room temperature technique whereas ALD requires growth at 300 °C. This limits the number of possible substrates. On the other hand, ALD can be done for large surface areas in one deposition run, and it can be used to deposit uniform films on very rough or even porous substrates, which is not possible for ion sputter deposition.

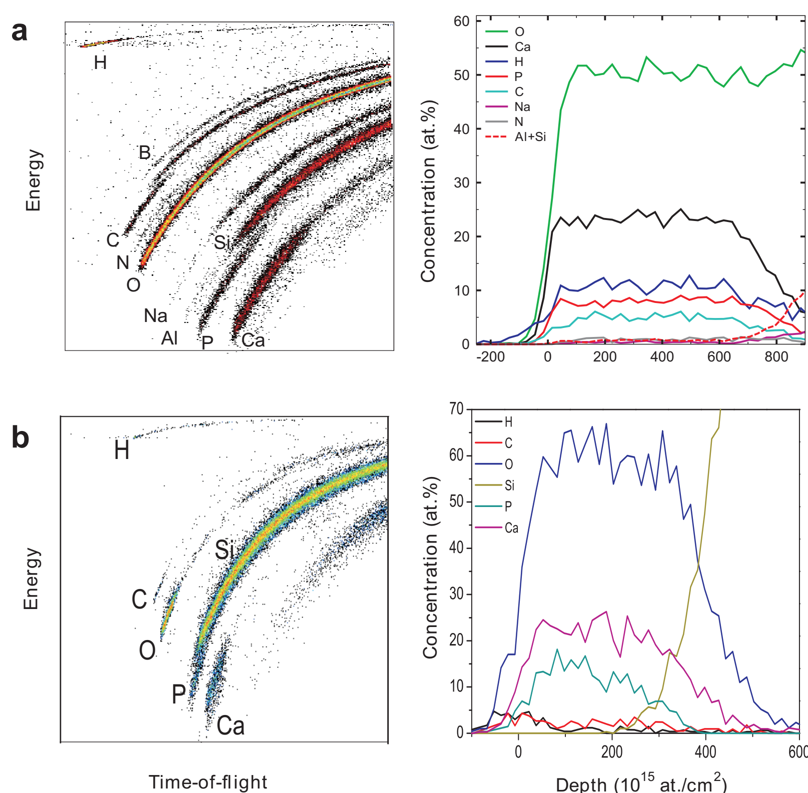

Figure 5.1: TOF–energy histogram and corresponding elemental depth profiles for a Ca-P-O thin film deposited using (a) ion sputter deposition on a borosilicate substrate and measured with 16 MeV $^{63}Cu^{7+}$ ions at IMEC (b) ALD on Si substrate measured with 11.9 MeV $^{63}Cu^{6+}$ ions at JYFL.

5.1.2 Annealing

As-deposited Ca-P-O films are amorphous for most thin film deposition techniques, and subsequent annealing is required to gain hydroxyapatite crystalline structure. In this thesis, sputter deposited Ca-P-O films were annealed in moist N_2 atmosphere for 10 min at 800 °C but X-Ray Diffraction measurements showed no crystalline peaks characteristic for HA. On the other hand, ALD Ca-P-O on Si substrate annealed at 800 °C showed nanocrystallite formation. TOF–ERDA showed a decrease in carbon and hydrogen content in ALD Ca-P-O film on Si substrates annealed at 600 °C and 700 °C, but an increase in hydrogen content was observed after annealing at 800 °C. This could originate from -OH groups formed during annealing in the presence of moist Ar atmosphere [68].

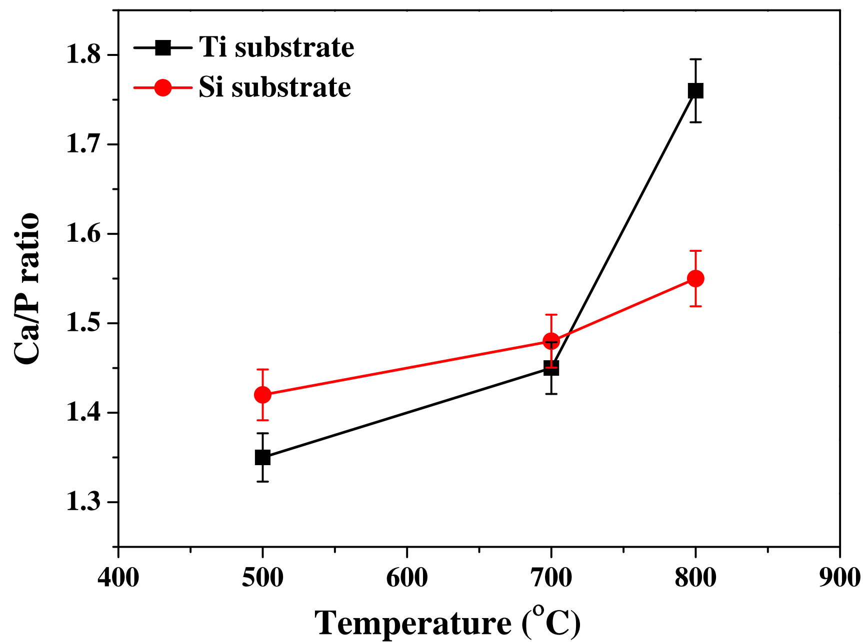

Figure 5.2: Ca/P atomic ratio of ALD Ca-P-O films on Si and Ti substrates abraded with 2000 grit size abrasive paper annealed for 10 minutes at 500 °C, 700 °C and 800 °C.

An increase in Ca/P atomic ratio was observed for annealed Ca-P-O films on Si and Ti substrates as shown in Fig. 5.2. In addition to crystallisation, this can be due to the volatile nature of phosphorus or weak phosphorus bonding in the films which can result in the formation of calcium rich film after the annealing process [103, 105].

A decrease in Ca and P areal densities in annealed Ca-P-O film on Ti substrates was noted, and this can be due to partial delamination of Ca-P-O film. Presence of Ti was observed at the surface of the sample after annealing at 800 °C whereas at 700 °C the Ca-P-O layer remained intact at the surface. Koch et al. studies suggest that HA films annealed at lower temperatures 575 °C exhibited better adhesion to Ti-6Al-4V substrates than films annealed at higher annealing temperature 700 °C. This can be attributed to softening of the Ti-6Al-4V substrate, formation of a titanium oxide layer between the HA film and the Ti-6Al-4V substrate, and thermal stresses [106].

5.1.3 Ion irradiation

The Ca/P ratios of low and high energy ion irradiated ALD Ca-P-O films were well within the range of the un-irradiated films, determined by means of RBS analysis. Reduction in film thickness due to low energy ion irradiation did not exceed 30% of the original thickness of 35 nm.

5.1.4 Substrate roughness

In TOF-ERDA both ingoing ions and out-coming sample atoms travel at glancing angle with respect to the surface. Because of this, the technique is surface roughness sensitive. In this work, special care was taken in the analysis to make sure that calculated values were comparable from one sample to another.

The ALD Ca-P-O films on abraded Ti substrates showed a decrease in Ca/P ratio with greater surface roughness as seen in Fig. 5.3. For a very smooth Si substrate the Ca/P atomic ratio was the highest. The difference in Ca/P ratios for abraded Ti and smooth Si substrates can be due to the following reasons: The growth mechanism of Ca-P-O film involves two processes, first the deposition of calcium carbonate and then successive $(Ch_3O)_3PO/H_2O$ cycles subsequently convert some of the carbonate to phosphate. The initial exchange reaction between carbonate and phosphate groups at the surface [68] of the substrate can lead to a dependence of Ca/P atomic ratio on the film thickness. Also during the deposition process a part of phosphorous precursor might adsorb to the substrate surface, which therefore alters the Ca/P atomic ratio. Film growth was faster on Ti substrates in comparison with Si substrate. This can be explained by larger surface area for abraded substrates during the first cycles, which leads to faster film growth. Also the oxidation of Ti and presence of hydroxyl group (-OH) creates the chemical difference during the deposition process. Since ALD is a chemical gas phase method relying only on surface reactions, the starting surface plays an important role in the first growth stages.

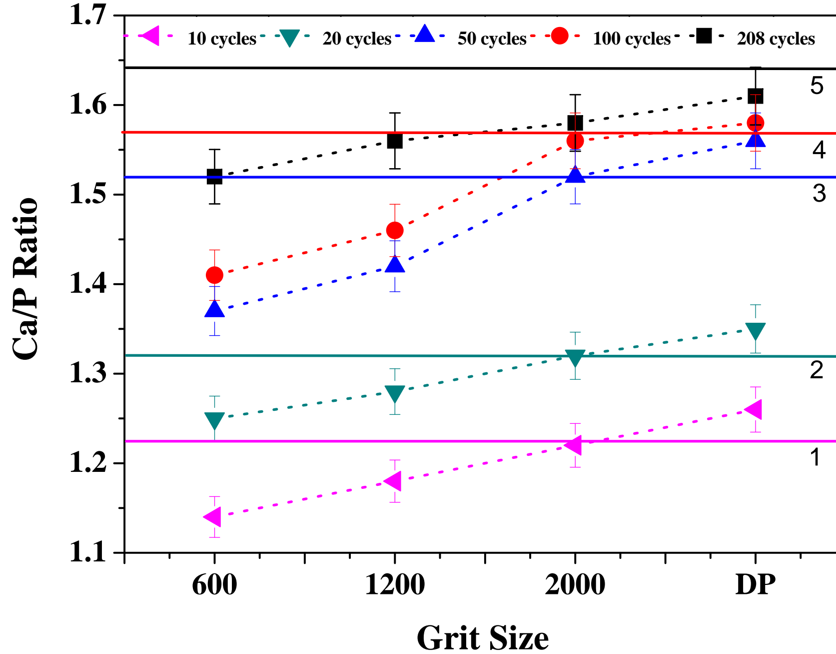

Figure 5.3: Ca/P atomic ratio of Ca-P-O films deposited with 10, 20, 50, 100 and 208 ALD cycles on Ti substrate abraded with SiC abrasive paper, grit size 600, 1200, 2000 and 3 μm diamond paste. The number denotes: (1) Film coated with 10 cycles, (2) 20 cycles, (3) 50 cycles, (4) 100 cycles, and (5) 208 cycles on Si substrate.

5.2 Surface morphology

In addition to the chemical environment, the surface morphology has an important role in determining the biocompatibility of a surface. The surface morphology was studied with an AFM with respect to annealing and ion irradiation of the as-deposited films. The amorphous as-deposited films followed the surface morphology of the substrate.

5.2.1 Annealing

Ca-P-O films were annealed in order to obtain crystalline structure similar to hydroxyapatite. The crystallisation process was clearly observed for ALD Ca-P-O film on Si substrate, as seen in Fig. 5.4. The film was very similar to the as-deposited one after annealing at 500 °C, but after annealing at 700 °C there were cracks at the surface, most likely resulting from the change in film density during crystallisation of the film or differences in thermal expansion coefficient between the Ca-P-O film and the Si substrate. After annealing at 800 °C the sample surface showed clear nanocrystallite (500 nm × 200 nm) formation perpendicular to the cracks.

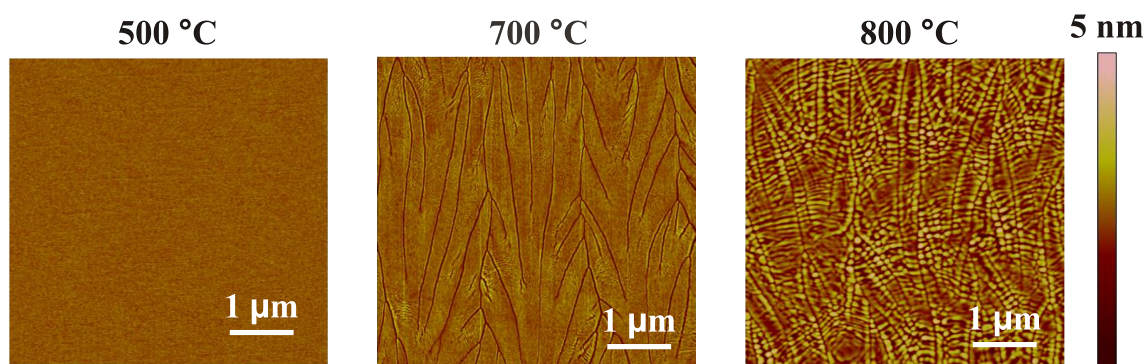

Figure 5.4: AFM images (5 μm×5 μm) of Ca-P-O films with 208 ALD cycles on Si substrates annealed under humid argon (99.999%) atmosphere for 10 minutes at 500 °C, 700 °C and 800 °C.

The AFM images of 208 ALD cycle Ca-P-O film deposited on abraded Ti substrates with 2000 grit paper and annealed at 500, 700, 800 °C are shown in Fig. 5.5. The surface of the sample annealed at 500 °C is similar to the one of as-deposited (not shown). Annealing at 700 °C lead to the crystallisation of the Ca-P-O film. A further temperature increase to 800 °C showed structures as high as 400 nm. These structures do not originate from the originally 50-60 nm thick Ca-P-O film but they are most likely TiO_2 crystals.

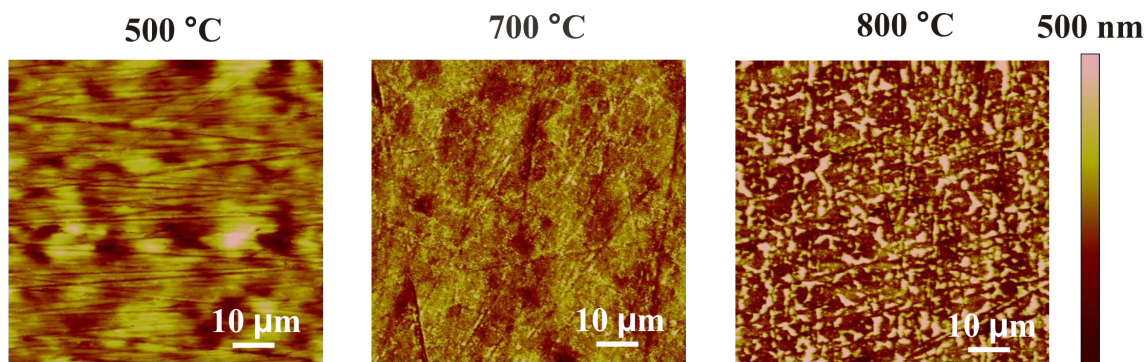

Figure 5.5: AFM images (75 μm×75 μm) of Ca-P-O films with 208 ALD cycles deposited on Ti substrates abraded with 2000 grit size abrasive paper and annealed for 10 minutes at 500 °C, 700 °C and 800 °C.

5.2.2 Ion irradiation effect

AFM images of annealed ALD Ca-P-O thin films before and after low energy ion irradiation are presented in Fig. 5.6. Low energy ion irradiation enhanced the lateral growth of a polycrystalline structure. This manifests itself as a change in surface morphology with the crystallites forming floral-like patterns around the nucleation sites. This effect is increased with an increase in ion acceleration energy. This can be either associated with Ostwald ripening which is governed by Gibbs-Thomson effect [107–109] or due to nuclear energy deposition from Ar ions. The ion bombardment contributes necessary atomic mobility from atomic displacements, giving rise to the floral patterns of the crystals.

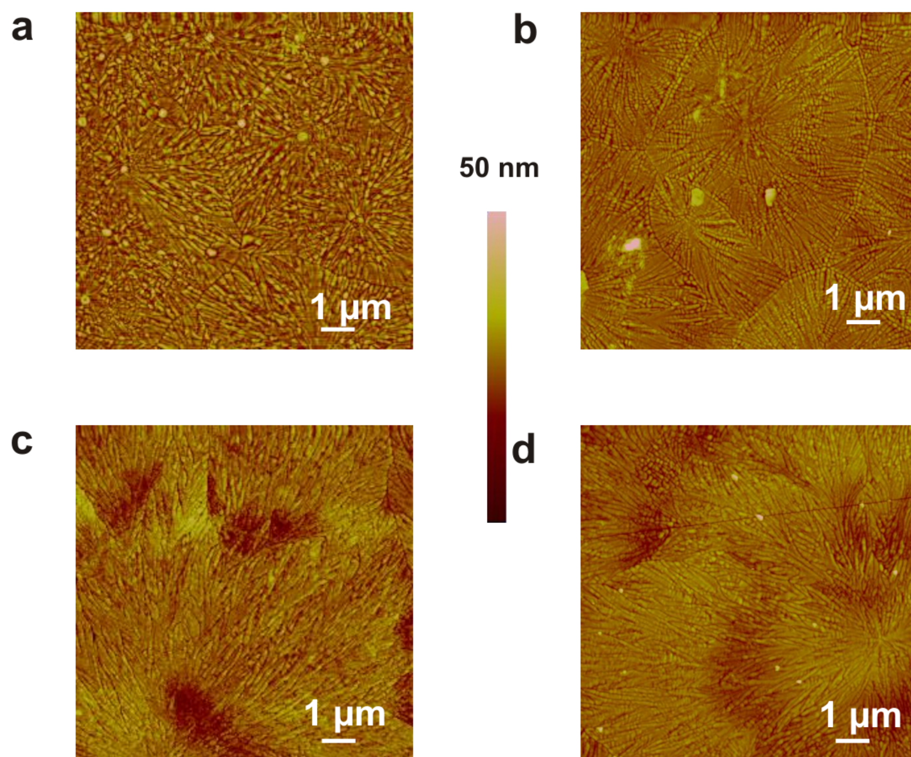

Figure 5.6: AFM images (10 μm×10 μm) of annealed Ca-P-O ALD films (a) un-irradiated surface and Ar beam irradiated at (b) 0.6 keV (c) 1 keV (d) 1.2 keV.

No floral crystallite patterns were observed on annealed films irradiated with 2 MeV $^{16}O^{+}$ beams. In contrast, the AFM images of the as-deposited samples showed a change in surface topography with the formation of raised islands of some 2-5 μm in diameter and 7 nm in height Fig. 5.7. This is most likely associated with the accumulation of residual gas in the blisters as a result of irradiation.

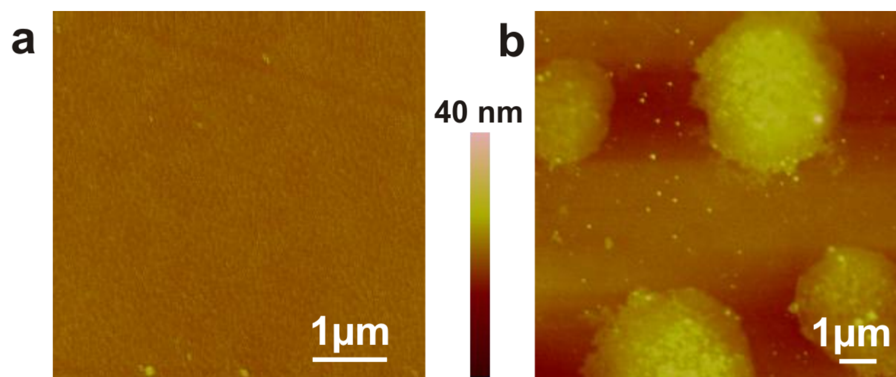

Figure 5.7: AFM images (5 μm×5 μm) of as-deposited ALD Ca-P-O (a) un-irradiated and (b) 2 MeV $^{16}O^{+}$ beam irradiated surface.

5.3 Hydrophilicity

Wetting properties are important for the interactions of cells with the surface. These were characterised in terms of the contact angle of a liquid drop. Fig. 5.8 shows energy vs contact angle for as-deposited and annealed Ca-P-O films after low energy ion irradiation. Post deposition annealing led to a decrease in contact angle from 72° to 55° for water and a decrease from 76° to 62° for cell culture medium. An increase in wettability after irradiation was noted, which was complemented with a significant overall reduction in contact angle for both as-deposited and annealed films. This significant change in contact angle can be associated with change in surface properties of Ca-P-O thin film such as sputter removal of the outer hydrocarbon layer, ion beam induced surface roughness and formation of reactive radicals. These reactive radicals play an important role in the formation of hydrophilic groups [110]. In contrast the Ca-P-O film bombarded with 2 MeV $^{16}O^{+}$ showed contradictory results with no reduction in the contact angle for both as-deposited and annealed films.

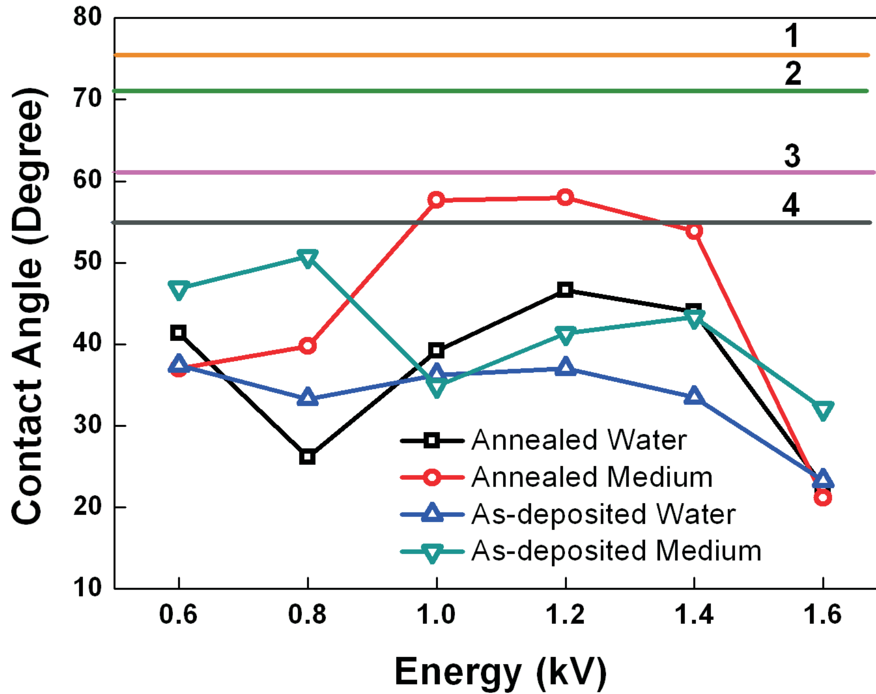

Figure 5.8: Energy vs contact angle for annealed and as-deposited Ca-P-O like films relative to deionised water and cell culture medium after low energy Ar irradiation, where the number represents: 1. un-irradiated as-deposited (medium), 2. un-irradiated as-deposited (water), 3. un-irradiated annealed (medium) and 4. un-irradiated annealed (water).

5.4 Crystalline phases

XRD results showed no diffraction peaks until annealing at 600 °C for as-deposited ALD Ca-P-O film on Si substrate. A few weak characteristic HA peaks were observed at 650 °C and above.

Strong diffraction peaks originating from titanium (∼35.1°, 38.4°, 40.2° and 53.0° at 2Θ) at 25 °C were observed on ALD Ca-P-O film on Ti and these peaks remain unchanged until 400 °C. Occurrence of the first trace of oxidation is observed at 500 °C with a weak diffraction peak at about 27.5° and broad peak at 38.1° as shown in Fig. 5.9. The diffraction peak at 38.4° indicates the formation of non-stoichiometric titanium oxide (TiO_{1-x}). At 600 °C this phase strengthens as those broad peaks can be observed on the side of every titanium peak. Moreover, the first weak peaks originating from stoichiometric titanium oxide (rutile form) can also be seen. In earlier study Holmberg et al. showed the existence of non-stoichiometric oxides of titanium [111].

The causes the broad peaks to emerge beside the titanium peaks as the hexagonal unit cell expanses in dynamical manner with an increase of oxygen content, until it eventually reaches to point where the lattice re-organises to stoichiometric oxide; a rutile's tetragonal crystal lattice in this case.

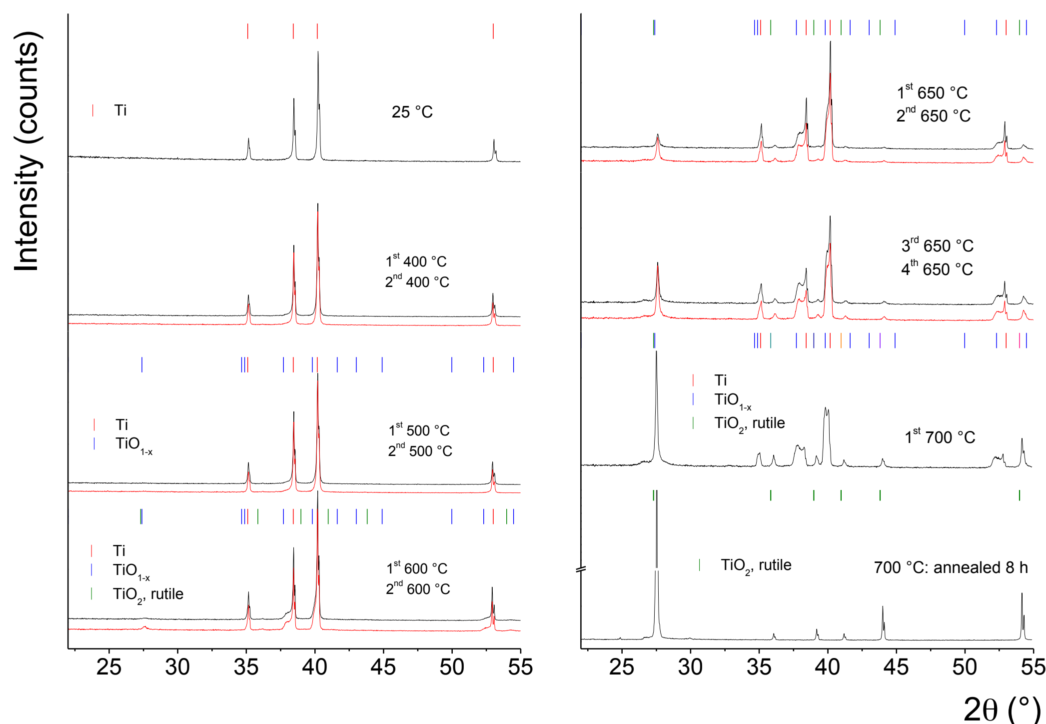

Figure 5.9: XRD patterns of Ca-P-O films on Ti substrate ground with 2000 grit size abrasive paper. The strongest diffraction peaks characteristic to Ti, TiO_{1-x} and TiO_2 (rutile) phases are indicated by the colored tick marks.

5.5 Cell growth and cell morphology

In this section, results are reported from in vitro pre-osteoblast cell culture assessments that have been investigated to associate responses from the Ca-P-O thin films. Post deposition annealing of Ca-P-O ALD films on Si substrate gave a decrease in contact angle and these films showed greater spreading of osteoblast-like cells after three hours of cell culture. A significant increase in cell spreading was observed after low energy ion irradiation for both as-deposited and annealed films. High energy ion irradiation on the other hand showed no significant difference after three hours of cell culture.

Fig. 5.10 presents the fluorescence microscope images from cell culture studies on Ti

substrates. After 24 hrs of cell culture the osteoblast showed more enhanced filopodia spreading on a Ti substrate polished with 3 μm diamond paste (Fig. 5.10 (b)) than on a Ti substrate abraded using SiC paper of grit size 600 (Fig. 5.10 (a)). No significant difference in cell spreading was noticed between the uncoated Ti control substrate and the ALD deposited Ti substrate. This suggests that difference in cell spreading is more due to the surface roughness than the effect of Ca/P atomic ratio on Ti substrates. Similarly Ti substrates annealed at 500 °C and 700 °C exhibited greater filopodia spreading of osteoblasts-like cells than the substrate annealed at 800 °C, which showed a reduced number of cells and rounded cell morphology. Stable adhesion with maximised cell proliferation have earlier been observed on moderately rough substrates [112]. Unlike amorphous films deposited using ion sputtering, as-deposited ALD film on titanium showed no dissolution of the Ca-P-O thin film in the cell growth medium. In studies of Thian et al., silicon-substituted hydroxyapatite films were deposited using magnetron co-sputtering on abraded Ti substrate. The films which were annealed at 700 °C for 3 hours under a moist Ar atmosphere demonstrated increased spreading and attachment of human osteoblast-like cells [113].

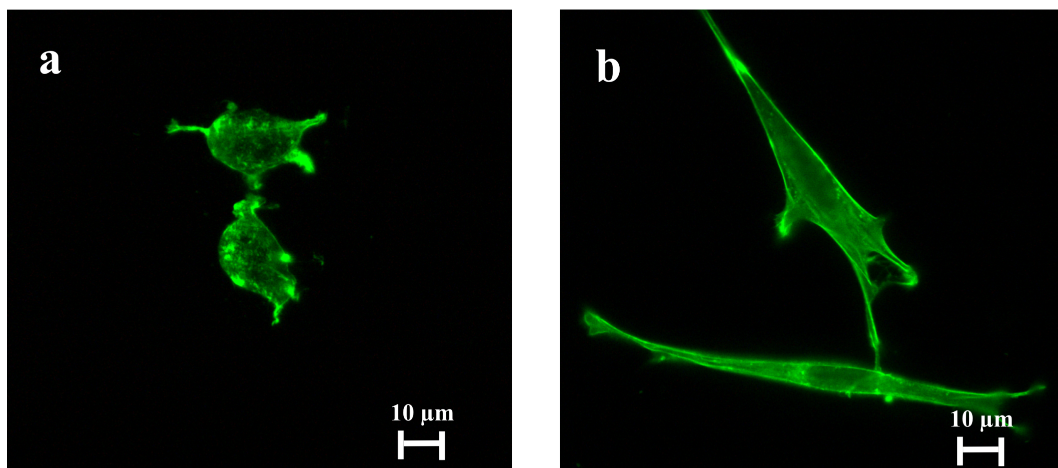

Figure 5.10: Fluorescence microscope images (140 μm × 120 μm) of mouse pre-osteoblast cells cultured on Ca-P-O films with 208 cycles on Ti substrates (a) abraded using 600 grit SiC abrasive paper b) polished using 3 μm diamond paste.

6 Conclusions

In this work the results from deposition, modification and characterisation of Ca-P-O thin films deposited using ion sputtering and ALD are presented. The general goal was to prepare thin biocompatible calcium phosphate films on substrates made of different materials and having different surface morphologies. Ion beams played a central role in this study. Ions were used both for modification and compositional characterisation of the films. The biocompatibility and surface topography of the films were probed by means of *in vitro* cell studies and atomic force microscopy, respectively.

Among the deposition techniques, ion sputtering deposition has the great advantage of being a room temperature technique. In this study a Ca/P ratio similar to that of hydroxyapatite could be reached by adding extra phosphorous to the sputtering target. The drawbacks of the technique were high film impurity content, lack of crystallisation during post-deposition high temperature annealing and dissolution of thin films in the cell culture medium.

The as-deposited ALD Ca-P-O films are amorphous, and high temperature post-deposition annealing was required for crystallisation. Ion irradiation of as-deposited films was tested as an alternative low-temperature process to mimic the energy deposition to the film during the annealing process. Low energy irradiation did not initiate any crystallite formation in as-deposited films, but improved the hydrophilicity of the thin film surfaces, as determined with contact angle measurements. Annealed and crystallised ALD Ca-P-O films showed an increase in hydrophilicity in comparison with as-deposited films, and this hydrophilicity was further improved by low energy ion irradiation.

Ca-P-O films were successfully deposited on Ti substrates with different roughnesses using ALD. The film growth and Ca/P ratio were studied for films aiming to be stoichiometric, as well as for clearly phosphorous rich films. The effect of substrate roughness was observed in the composition of deposited films, an increase in Ca/P atomic ratio was observed with decrease in substrate roughness. In the cell tests with mouse pre-osteoblast cells the ALD Ca-P-O films showed preferential filopodic growth on smoother surfaces as compared to rough surfaces. The presence of an ALD film on the surface or lower temperature annealing did not have great influence on the number of cells or morphology. This similarity is due to the biocompatible nature of Ti and its amorphous oxides. The high temperature annealing at 800 °C was required for the formation of nanocrystallites on Ca-P-O films on Si, and pronounced filopodia

structures of cells were observed on these films. Annealing at the same temperature caused a major change in the Ti sample surface topography due to oxidation of the substrate. This resulted in rounded cell morphology with a greatly reduced the number of pre-osteoblast cells on the annealed surface.

Atomic layer deposition is more versatile technique than the ion sputtering method for depositing Ca-P-O films. It has many advantages such as low dissolvability of films in cell culture medium, uniform deposition, tunable Ca/P atomic ratio and ability to deposit on complex and porous structures. One interesting idea for future research could be to use heavy water instead of normal water during the ALD process or post deposition annealing, and this way trace the origin of hydrogen in the films.

References

[1] M. Jarcho, Clin. Orthop. Relat. Res. 157 (1981) 259.

[2] A. L. Oliveira, J. F. Mano, R. L. Reis, Curr. Opin. Solid. St. M. 7 (2003) 309.

[3] G. Heimke, P. Griss, Med. and Bio. Eng. and Comput. 18 (1980) 503.

[4] C. J. Damien, J. R. Parsons, J. Appl. Biomate. 2 (1991) 187.

[5] M. Bohner, Eur. Spine. J. 10 (2001) 114.

[6] W. L. Jaffe, D. F. Scott, N. Y. N. York, J. Bone Joint Surg. 78 (1996) 1918.

[7] A. Wisbey, P. J. Gregson, M. Tuke, Biomaterials 8 (1987) 477.

[8] C. Sella, J. C. Martin, A. Lechanu, J. Lecoeur, J. P. Bellier, M. F. Harmand, A. Naji, J. P. Davidas, Surf. Coat. Technol. 45 (1991) 129.

[9] M. Skirkhanzadeh, J. Mater. Sci-Mater. Med. 3 (1992) 322.

[10] R. P. Renz, A. Cunha, G. Wantowski, E. Blando, R. Hübler, Rev. Clín. Pesq. Odontol. 3 (2007) 149.

[11] L. L. Guéhennec, A. Soueidan, P. Layrolle, Y. Amouriq, Dent. Mater. 23 (2007) 844.

[12] L. Sun, C. C. Berndt, K. A. Gross, A. Kucuk, J. Biomed. Mater. Res. 5 (2001) 570.

[13] M. Akao, H. Aoki, K. Kato, J. Mater. Sci. 16 (1981) 809.

[14] P. Pingle, *Analytical Modeling of Hard Biocomposities*, , Phd thesis, University of Massachusetts Lowell (2008).

[15] C. Chu, X. Xue, J. Zhu, Z. Yin, J. Mater. Sci. Mater. Med. 15 (2004) 665.

[16] L. Sun, C. C. Berndt, K. A. Gross, A. Kucuk, J. Biomed. Mater. Res. 5 (2001) 570.

[17] C. W. Yang, T. S. Lui, Mater. Trans. 48 (2007) 211.

[18] O. Rahbek, S. Overgaard, M. Lind, K. Bendix, C. Bünger, K. Søballe, J. Bone Joint Surg. [Br] 83 (2001) 441.

[19] K. A. Gross, N. Ray, M. Røkkum, J. Biomed. Mater. Res. 2 (2002) 106.

[20] L. L. Hench, J. Am. Ceram. Soc. 7 (1998) 1705.

[21] R. Z. LeGeros, Ado. Dent. Res. 2 (1988) 164.

[22] R. G. T. Geesink, K. D. Groot, C. P. A. T. Klein, J Bone Joint Surg. [Br] 70 (1988) 217.

[23] R. I. Martin, P. W. Brown, J. Biomed. Mater. Res. 3 (1997) 299.

[24] I. H. Arita, V. M. Castano, D. S. Wilkinson, J. Mater. Sci. Mater. Med. 1 (1995) 19.

[25] J. M. Akao, H. Aoki, K. Kato, J. Mater. Sci. 3 (1981) 809.

[26] L. B. Kong, J. Ma, F. Boey, J. Mater. Sci. 6 (2002) 1131.

[27] X. Zhang, K. S. Vecchio, J. Cryst. Growth 1 (2007) 133.

[28] J. Wang, L. L. Shaw, J. Mater. Sci. Mater. Med. 20 (2009) 1223.

[29] Y. Yang, J. L. Ong, J. Tian, J. Appl. Phys. 21 (2002) 67.

[30] R. Xin, Y. Leng, J. Chen, Q. Zhang, Biomaterials 26 (2005) 6477.

[31] R. J. Kingsley, R. V. Gilder, R. Z. Legeros, N. Watanabe, J. Phycol. 39 (2003) 937.

[32] Y. C. Tsui, C. Doyle, T. W. Clyne, Biomaterials 19 (1998) 2015.

[33] K. Soballe, S. Overgaard, J. Bone Joint Surg. 78 (1996) 689.

[34] Y. Yang, K. H. Kim, J. L.Ong, Biomaterials 26 (2005) 327.

[35] D. A. Puleo, A. Nanci, Biomaterials 20 (1999) 2311.

[36] K. J. L. Burg, S. Porter, J. F. Kellam, Biomaterials 21 (2000) 2347.

[37] G. Carotenuto, G. Spagnuolo, L. Ambrosio, L. Nicolais, J. Mater. Sci. Mater. Med. 10 (1999) 671.

[38] P. K. Bajpai, H. A. Benhuzzi, J. Biomed. Mater. Res. 22 (1998) 1245.

[39] A. Barroug, J. Fastrez, J. Lemaitre, P. G. Rouxhet, J. Colloid. Interface Sci. 189 (19987) 37.

[40] A. Barroug, M. J. Glimcher, J. Orthop. Res. 20 (2002) 280.

[41] D. Perozzollo, W. R. Lacefiled, D. M. B. and, J. Biomed. Mater. Res. 22 (1998) 1245.

[42] M. Wei, A. J. Ruys, M. V. Swain, S. H. K. B. K. Milthorpe, C. C. Sorrell, J. Mater. Sci. Mater. Med. 10 (1999) 401.

[43] L. Tang, C. Tsaiff, W. W. Gerberich, L. Kruckebeu, D. R. Kania, Biomaterials 16 (1995) 485.

[44] X. Liu, P. K. Chu, C. Ding, Mater. Sci. Eng. R. 47 (2004) 49.

[45] B. Leffler, *STAINLESS - stainless steels and their properties.*, from and http://www.outokumpu.com/files/Group/HR/Documents/STAINLESS20.pdf.

[46] S. S. I. of North America, *Chemical and Physical properties of Stainless Steel.*, http://www.ssina.com/composition/chemical.html.

[47] B. D. Boyan, T. W. Hummert, D. D. Dean, Z. Schwartz, Biomaterials 17 (1996) 137.

[48] C. Larsson, P. Thomsen, B. O. Aronsson, M. Rodahl, J. Lausmaa, B. Kasemo, L. E. Ericson, Biomaterials 17 (1996) 605.

[49] R. G. Flemming, C. J. Murphy, G. A. Abrams, S. L. Goodman, P. F. Nealey, Biomaterials 20 (1999) 573.

[50] B. D. Boyan, T. W. Hummert, D. D. Dean, Z. Schwartz, Biomaterials 17 (1996) 137.

[51] C. Larsson, P. Thomsen, B. O. Aronsson, M. Rodahl, J. Lausmaa, B. Kasemo, L. E. Ericson, Biomaterials 17 (1996) 605.

[52] P. Klokkevold, R. Nishimure, M. Adachi, Clin. Oral Implant Res. 8 (1997) 442.

[53] D. Y. Sullivan, R. L. Sherwood, T. N. Mai, J. Prosthet. Dent. 78 (1997) 379.

[54] A. Wennerberg, C. Hallgren, C. Johansson, Clin. Oral Implants Res. 9 (1998) 11.

[55] I. Ericsson, C. B. Johansson, H. Bystedt, Clin. Oral Implants Res. 5 (1994) 202.

[56] Goodfellow http://www.goodfellow.com/.

[57] SIGMA-ALDRICH from: http://www.sigmaaldrich.com.

[58] R. Behrich, *Topics in Applied Physics (52) Sputtering by Particle Bombardment II - Sputtering of Alloys and Compounds and Electron and Neutron Sputtering and Surface Topography*, Springer-Verlag, Berlin, 1981.

[59] H. H. Andersen, *Ion Implantation and Beam processing*, J.S. Williams and J.M. Poate and Academic Press, London.

[60] R. Behrich, *Topics in Applied Physics (52) Sputtering by Particle Bombardment I - Sputtering of Single-Element Solidy*, Springer-Verlag, Berlin, 1981.

[61] K. van Dijk, H. G. Schaeken, J. G. C. Wolke, J. A. Jansen, Biomaterials 17 (1996) 405.

[62] J. L. Ong, L. C. Lucas, W. R. Lacefield, E. D. Rigney, Biomaterials 13 (1992) 249.

[63] S. J. Ding, C. P. Ju, J. H. C. Lin, J. Biomed. Mater. Res. 44 (1999) 266.

[64] P. Laitinen, M. Nevala, A. Pirojenko, K. Ranttila, R. Seppälä, I. Riihimäki, J. Räisänen, A. Virtanen, Nucl. Instr. and Meth. in Phys. Res. B 226 (2004) 441.

[65] M. Leskelä, M. Ritala, Thin Solid Films 409 (2002) 138.

[66] S. M. George, Chem. Rev. 110 (2010) 111.

[67] M. Leskelä, M. Ritala, Thin solid films 409 (2002) 138.

[68] M. Putkonen, T. Sajavaara, P. Rahkila, L. Niinistö, S. Cheng, H. J. Whitlow, Thin Solid Films 517 (2009) 5819.

[69] S. K. Bhateja, E. H. Andrews, R. J. Young, J. Polym. Sci. B 25 (1987) 717.

[70] N. J. Chou, D. W. Dong, J. Kim, A. C. L. and, J. Electrochem. Soc. Solid State Sci. Technol. 131 (1984) 2335.

[71] A. J. Kellock, G. L. Nyberg, J. S. Williams, Vacuum 35 (1985) 625.

[72] S. R. Forrest, M. L. Kaplan, P. H. Schmidt, T. Venkatesan, A. J. Lovinger, Appl. Phys. Lett. 41 (1982) 708.

[73] O. Puglisi, A. Licciardello, L. Calcagno, G. Foti, Nucl. Instr. and Meth. in Phys. Res. B 19/20 (1987) 865.

[74] R. Hellborg, H. J. Whitlow, Y. Zhang, *Ion Beams in Nanoscience and Technology*, 2009.

[75] P. Sigmund, *Stopping of Heavy Ions A Theoretical Approach*, Springer, Berlin, 2004.

[76] P. Sigmund, *Particle penetration and radiation effects*, Springer, Berlin, 2006.

[77] M. Nastasi, J. W. Mayer, J. K. Hirvonen, *Ion-solid Interaction: Fundamentals and Applications*, Cambridge University Press, New York, 1996.

[78] S. Gorelick, T. Ylimäki, T. Sajavaara, M. Laitinen, A. R. A. Sagari, H. J. Whitlow, Nucl. Instr. and Meth. in Phys. Res. B 260 (2007) 77.

[79] S. Gorelick, T. Sajavaara, M. Laitinen, N. Puttaraksa, H. J. Whitlow, Mater. Res. Soc. Symp. Proc. 1020–GG03–04.

[80] S. Gorelick, *MeV Ion Beam Lithography of High Aspect Ratio Structures With a Focused or Aperture–shaped Beam for Applications in Biomedical Studies and Microfludics*, , Phd thesis, University of Jyväskylä (2008).

[81] N. Puttaraksa, S. Gorelick, T. Sajavaara, M. Laitinen, S. Singkarat, H. J. Whitlow, J. Vac. Sci. Tech. B 26 (2008) 1732.

[82] J. Frantz, J. Tarus, K. Nordlund, J. Keinonen, Phys. Rev. B 12 (2001) 1.

[83] M. W. Bench, I. M. Robertson, M. A. Kirk, Nucl. Instrum. Methods Phys. Res. B 59/60 (1991) 372.

[84] M. W. Bench, I. M. Robertson, M. A. Kirk, I. Jencic, J. Appl. Phys. 87 (2000) 49.

[85] I. Jencic, M. W. Bench, I. M. Robertson, M. A. Kirk, J. Appl. Phys. 78 (1995) 974.

[86] R. Hellborg, *Electrostatic Accelerator*, Springer, Berlin and Heidelberg and New York, 2005.

[87] D. Buune, R. Hellborg, H. J. Whitlow, O. Hunderi, *Surface Characterization*, Wiley-VCH, Weinheim and Berlin and New York and Chichester and Brisbane and Singapore and Toronto, 1997.

[88] H. J. Whitlow, G. Possnert, C. S. Petersson, Nucl. Instr. and Meth. in Phys. Res. B 27 (1987) 448.

[89] J. R. Tesmer, M. Nastasi, *Handbook of Modern Ion Beam Materials Analysis*, Materials Research Society, Pittsburgh and Pennsylvania, 1995.

[90] S. Giangrandi, T. Sajavaara, B. Brijs, K. Arstila, A. Vantomme, W. Vandervorst, Nucl. Instr. and Meth. in Phys. Res. B. 266 (2008) 5144.

[91] M. Laitinen, T. Sajavaara, M. Rossi, J. Julin, R. L. Puurunen, T. Suni, T. Ishida, H. Fujita, K. Arstila, B. Brijs, H. J. Whitlow, Nucl. Instr. and Meth. in Phys. Res. B 269 (2011) 3021.

[92] T. Sajavaara, K. Arstila, A. Laakso, J. Keinonent, Nucl. Instr. and Meth. in Phys. Res. B. 161-163 (2000) 235.

[93] V. J. Morris, A. R. Kirby, A. P. Gunning, *Atomic Force Microscopy for Biologist*, Imperial College Press, London, 2010.

[94] Micromasch from: http://www.spmtips.com/probes/1l.

[95] H. P. Klug, L. E. Alexander, *X-ray Diffraction Procedures for Polycrystalline and Amorphous Materials*, John Wiley and Sons, Inc., New York, 1954.

[96] M. Chasse, G. G. Ross, Nucl. Instr. and Meth. in Phys. Res. B 193 (2002) 835.

[97] L. Hanley, S. B. Sinnott, Surface Science 500 (2002) 500.

[98] D. Quéré, Annu. Rev. Mater. Res. 38 (2008) 71.

[99] T. Turpeinen, M. Myllys, J. Timonen, K. Majavara, T. Kärkkäinen, manuscript.

[100] α MEM (1X) (22571-020) from http://www.invitrogen.com.

[101] G. Invitrogen https://www.lifetechnologies.com/us/en/home.html.

[102] W. S. Rasband, ImageJ, U. S. National Institutes of Health. (1997-2011) http://imagej.nih.gov/ij/.

[103] K. van Dijk, H. G. Schaeken, J. G. C. Wolke, J. A. Jansen, Biomaterials 17 (1996) 405.

[104] T. F. Stoica, C. Morosanu, A. Slav, T. Stoica, P. Osiceanu, C. Anastasescu, M. Gartner, M. Zaharescu, Thin Solid Films 516 (2008) 8112.

[105] C. X. Wang, Z. Q. Cheng, M. Wang, Z. Y. Liu, P. L. Wang, J. Biomed. Mater. Res. 55 (2001) 587.

[106] C. F. Koch, S. Johnson, D. Kumar, M. Jelinek, D. B. Chrisey, A. Doraiswamy, C. Jin, R. J. Narayane, I. N. Mihailescu, Mat. Sci. Eng. C 27 (2007) 484.

[107] A. Romanyuk, V. Spassov, V. Melnik, J. Appl. Phys. 99 (2006) 034314.

[108] C. Liu, A. Wenzel, H. Riechert, B. Rauschenbach, From Ion Implantation Proceeding 2 (1999) 881.

[109] D. H. Lowndes, From the Proceeding of third symposium on advanced photon processing and measurements technology (2000) 232.

[110] W. W. Choi, S. K. Koh, H. J. Jung, J. Vac. Sci. Technol. A 14 (1996) 2366.

[111] B. Holmberg, Acta Chem Scandinavia 16 (1962) 1245.

[112] F. Gentile, L. Tirinato, E. Battista, F. Causa, C. Liberale, E. M. D. Fabrizio, P. Decuzzi, Biomaterials 31 (2010) 7205.

[113] E. S. Thian, J. Huang, S. M. Best, Z. H. Barber, W. Bonfield, Biomaterials 26 (2005) 2947.